All silicon lithium-ion batteries

Licentiate thesis

Chao Xu

Department of Chemistry – Ångström Laboratory
Uppsala Univeristy

Abstract

Lithium-ion batteries have been widely used as power supplies for portable electronic devices due to their higher gravimetric and volumetric energy densities compared to other electrochemical energy storage technologies, such as lead-acid, Ni-Cd and Ni-MH batteries. Developing a novel battery chemistry, ‘‘all silicon lithium-ion batteries’’, using lithium iron silicate as the cathode and silicon as the anode, is the primary aim of this Ph.D project. This licentiate thesis is focused on improving the performance of the silicon anode via optimization of electrolyte composition and electrode formulation. Fluoroethylene carbonate (FEC) was investigated as an electrolyte additive for silicon composite electrodes, and both the capacity retention as well as coulombic efficiency were significantly improved by introducing 10 wt% FEC into the LP40 electrolyte. This is due to the formation of a stable SEI, which mainly consisted of FEC decomposition products of LiF, -CHF-OCO_2-, etc. The chemical composition of the SEI was identified by synchrotron radiation based photoelectron spectroscopy. This conformal SEI prevented formation of large amounts of cracks and continues electrolyte decomposition on the silicon electrode. An alternative lithium salt, lithium 4,5-dicyano-2-trifluoromethanoimidazole (LiTDI), was studied with the silicon electrode in this thesis. The SEI formation led to a rather low 1st cycle coulombic efficiency of 44.4%, and the SEI layer was found to contain hydrocarbon, ether-type and carbonate-type species. Different to conventional composite silicon electrodes, which require heavy and expensive copper current collector, a flexible silicon electrode, consisted of only silicon nanopowder, *Cladophora* nanocellulose and carbon nanotube, was facilely prepared via vacuum filtration. The electrode showed good mechanical, long-term cycling as well as rate capability performance.

List of Papers

This thesis is based on the following papers, which are referred to in the text by their Roman numerals.

I. **Improved Performance of Silicon Anode for Li-Ion Batteries: Understanding the Surface Modification Mechanism of Fluoroethylene Carbonate as an Effective Electrolyte Additive**
Chao Xu, Fredrik Lindgren, Bertrand Philippe, Mihaela Gorgoi, Fredrik Björefors, Kristina Edström, Torbjörn Gustafsson
Chemistry of materials **27**, 2591–2599, 2015

II. **A hard X-ray photoelectron spectroscopy study on the solid electrolyte interphase of a lithium 4,5-dicyano-2-(trifluoromethyl)imidazolide based electrolyte for Si-electrodes**
Fredrik Lindgren, Chao Xu, Anna Andersson, Kristina Edström, Torbjörn Gustafsson, Fredrik Björefors
In manuscript

III. **Flexible freestanding *Cladophora* nanocellulose paper based Si anodes for lithium-ion batteries**
Zhaohui Wang, Chao Xu, Petter Tammela, Jinxing Huo, Torbjörn Gustafsson, Kristina Edström, Maria Strømme Leif Nyholm
Journal of Materials Chemistry A **3**, 14109-14115, 2015

Comments on my contribution to this work:

I. Planed and performed most of the experimental work (sample preparation, electrochemical tests, PES measurements and analysis). Wrote the manuscript and took part in all discussions throughout the paper editing.

II. Involved in planning and performed PES measurements. Took part in all discussions.

III. Involved in planning and performed part of the experimental work (battery assembly and electrochemical tests). Wrote part of the manuscript and took part in all discussions

The following papers are not included in this thesis:

I. Interface layer formation in solid polymer electrolyte lithium batteries: an XPS study
Chao Xu, Bing Sun, Torbjörn Gustafsson, Kristina Edström, Daniel Brandell, Maria Hahlin
Journal of Materials Chemistry A **2**, 7256-7264, 2014

II. At the polymer electrolyte interfaces: the role of the polymer host in interphase layer formation in Li-batteries
Bing Sun, Chao Xu, Jonas Mindemark, Torbjörn Gustafsson, Kristina Edström, Daniel Brandell
Journal of Materials Chemistry A **3**, 13994-14000, 2015

III. Conducting Polymer Paper-Based Cathodes for High Areal Capacity Lithium-Organic Batteries
Zhaohui Wang, Chao Xu, Petter Tammela, Peng Zhang, Kristina Edström, Torbjörn Gustafsson, Maria Strømme, Leif Nyholm
Energy Technology **3**, 563-569, 2015

IV. A novel HPXPS experimental method for characterization of the interface between a solid electrode and electrolyte demonstrated with a Li-ion battery system
Julia Maibach, Chao Xu, Susanna K. Eriksson, John Åhlund, Torbjörn Gustafsson, Hans Siegbahn, Håkan Rensmo, Kristina Edström, Maria Hahlin
Review of Scientific Instruments **86**, 044101, 2015

Contents

Abbreviations

AFM	Atomic force microscopy
CMC	Carboxymethyl cellulose
CNC	*Cladophora* nanocellulose
CNT	Carbon nanotube
DEC	Diethyl carbonate
DMC	Dimethyl carbonate
EC	Ethylene carbonate
EIS	Electrochemical impedance spectroscopy
EMC	Ethylmethyl carbonate
FEC	Fluoroethylene carbonate
FT-IR	Fourier transform infrared spectroscopy
LCO	Lithium cobalt oxide
LIB	Lithium-ion battery
Li2DFB	Dilithium dodecafluorododecaborate
LiDFOB	Lithium difluorooxalatoborate
LiFSI	Lithium bis(fluorosulfonyl)imide
LiTDI	Lithium 4,5-dicyano-2-trifluoromethanoimidazole
LFP	Lithium iron phosphate
LFS	Lithium iron silicate
LMO	Lithium manganese oxide
LNMO	Lithium nickel manganese oxide
NCA	Lithium nickel cobalt aluminum oxide
NMC	Lithium nickel manganese cobalt oxide
OCV	Open circuit voltage
PAA	Poly(acrylic acid)
PES	Photoelectron spectroscopy
PVdF	Polyvinylidene fluoride
SEI	Solid electrolyte interphase
SEM	Scanning electron microscopy
TEM	Transmission electron microscopy
TOF-SIMS	Time of flight-secondary ion mass spectroscopy
VC	Vinylene carbonate
XPS	X-ray photoelectron spectroscopy

1. Introduction

1.1 Lithium-ion batteries

As the consumption and performance of portable electronic devices, such as mobile phones, laptops, etc., have significantly increased over the past decades, power supplies with higher volumetric as well as gravimetric energy density are strongly needed. Among the commercialized electrochemical energy storage technologies, lithium-ion batteries (LIBs) provide the highest energy density as illustrated in *Figure 1(a)*, compared to lead acid, Ni-Cd, Ni-MH batteries.[1] Since the commercialized by Sony in 1991,[2] LIBs have dominated the power supply market for portable electronic devices. Moreover, replacing traditional petroleum fuels in vehicles is another important driving force of developing advanced LIBs for electric vehicles, in order to reduce the use of limited fossil fuel as well as carbon dioxide emission.

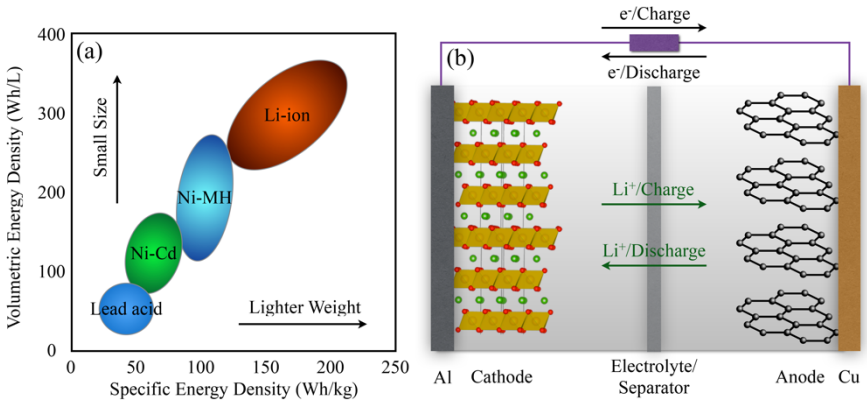

Figure 1. (a) A Comparison of the rechargeable battery technologies as a function of volumetric and specific energy density. Redrawn from ref.[1] (b) A Schematic representation of the working principle of a lithium-ion battery.

Conventional rechargeable lithium-ion batteries mainly consist of two composite electrodes (cathode and anode) and a Li^+ ion conducting electrolyte (an additional separator is required for liquid electrolytes). LIBs are also referred as rocking-chair batteries since Li^+ moves between the two electrodes during cycling as demonstrated in *Figure 1(b)*. During charging, the cathode material is oxidized, and Li^+ is extracted (delithiation) and moves to

the anode. The reactions are reversed during discharging and the Li^+ moves from the anode to the cathode through the electrolyte.

1.2 Electrode materials

1.2.1 Cathode materials

$LiCoO_2$ (LCO) was used as the cathode material in the first commercialized lithium-ion battery by Sony in 1991.[3] The layered structured $LiCoO_2$ can be reversibly cycled with half of the Li inventory, giving a theoretical capacity of 150 mAh/g with an average cycling voltage of 3.9 V (vs. Li^+/Li, all potentials stated in this text are, unless specifically stated, measured versus the Li^+/Li redox couple.).[4,5] However, $LiCoO_2$ suffers from issues such as high cost and toxicity of cobalt as well as the safety hazard from O_2 evolution after over-charging.[6,7] Metal (Mn, Ni and/or Al) substitution of Co to form layer-structured lithium metal oxide solid solutions, such as $Li(Ni,Mn,Co)O_2$ (NMC), $Li(Ni,Co,Al)O_2$ (NCA), is found to be beneficial to the thermal stability, cyclability and rate capability for $LiCoO_2$-based cathode materials.[8-10] Lithium-rich layer oxides, commonly denoted as $(1-y)Li_2MnO_3 \cdot yLiMO_2$ (M = Mn, Co, Ni), has been particularly attracting currently due to their high energy density (gravimetric density of ~ 250 mAh/g , average voltage of ~ 3.7 V).[11-13] Spinel $LiMn_2O_4$ (LMO) is also one of the first developed cathode materials for rechargeable LIBs, and has a significant advantage in cost compared to $LiCoO_2$ cathode.[14-16] However, the cyclability of $LiMn_2O_4$ is rather poor as Mn^{2+} (formed through disproportionation $2Mn^{3+} \rightarrow Mn^{2+} + Mn^{4+}$) tends to be dissolved into the electrolyte.[16] One attractive spinel derivate, $LiNi_{0.5}Mn_{1.5}O_4$ (LNMO), exhibits a high operating voltage of ~ 4.7 V. This, however, seriously challenges the stability of the conventional carbonate-based liquid electrolyte.[17,18] $LiFePO_4$ (LFP) is another cathode material widely used in today's commercialized lithium-ion batteries due to its excellent structural stability, decent capacity (~ 160 mAh/g) and cycling voltage (~ 3.5 V).[19-21] Olivines-structured $LiFePO_4$ has been well studied since the first report in 1997 and tremendous amount of effort has been devoted to overcome its intrinsic problems of poor electronic and ionic conductivity.[19,21-23]

Lithium metal silicate (Li_2MSiO_4, M = Fe, Mn, etc.) is a relatively new class of cathode materials, and Nytén firstly synthesized and investigated Li_2FeSiO_4 (LFS, theoretical capacity of 166 mAh/g, based on one lithium ion reaction per formula unit) in 2005.[24,25] The potential of extracting two lithium ions per formula unit, which gives a theoretical capacity as high as ~ 330 mAh/g, is one of the most attracting features of LFS cathode materials. Besides, the strong Si-O bonding can result in good electrochemical and

chemical stability, and the use of earth abundant elements (Fe/Mn, Si) could also potentially reduce the cost of the material.[24] Three different crystal systems of Li_2FeSiO_4, which are orthorhombic (space group *Pmn2$_1$*), monoclinic (space group *P2$_1$*) and orthorhombic (space group *Pmnb*) have been reported in the literature so far, and different synthesis methods and conditions can significantly influence the structure of the product.[24,26,27] Various synthetic methods, such as solid-state, sol-gel, combustion, hydrothermal, hydrothermal assisted sol-gel, have been explored to synthesize Li_2FeSiO_4.[24,27-33] The electrochemical performance of the Li_2FeSiO_4 was first investigated by Nytén, and the charge and discharge potential plateaus during the first cycle were reported at 3.10 V and 2.76 V, respectively (at 60 °C).[24,25] A shift from 3.10 V to 2.80 V in charge potential plateau was observed from the first cycle to the following cycles and it is due to the rearrangement of the structure during the first cycle. Although the electrochemical behavior of Li_2FeSiO_4 to some extent differs from different synthesis routes, this change in charge potential from the first to the second cycles appears to be a common feature.[25,28-30,32,33] The surface chemistry on Li_2FeSiO_4 electrode has also been studied, showing better salt stability of $LiN(SO_2CF_3)_2$ than $LiPF_6$ upon cycling.[34,35] Investigations on the aging of Li_2FeSiO_4 suggested that Li_2FeSiO_4 would degrade to Li_2SiF_6 in the fluorine-based electrolyte at elevated temperature.[36]

Unlike Li_2FeSiO_4, for which it is difficult to extract more than one lithium ion per formula unit, Li_2MnSiO_4 is more promising in the aspect of potentially obtaining high energy density, due to moderate voltages of $Mn^{2+/3+}$ and $Mn^{3+/4+}$ electrochemical couples.[37] However, Li_2MnSiO_4 is reported to be inherently unstable upon delithiation and its structure tends to collapse. Stabilization with partial metal ion substitution (e.g. Fe, Ni) for Mn has been proposed and studied, but the electrochemical performance is rather limited and still needs to be improved.[37-40]

1.2.2 Anode materials

Different from cathode materials, most of which are insertion compounds, anode materials for rechargeable lithium-ion batteries can be generally divided into three classes based on different lithiation/delithiation mechanisms: intercalation, alloying and conversion materials.

1.2.2.1 Intercalation materials

Graphite, which is an intercalation material allows insertion and removal of lithium between the graphene sheets, is the most commonly used anode material in today's commercialized lithium-ion batteries. Graphite has a theoretical capacity of 372 mAh/g which corresponds to the composition of LiC_6 at fully lithiated state.[41] The low average working potential of ~ 0.125 V is one of the advantages for the use of graphite as an anode material in lithium-

ion batteries. However, due to the instability of the organic liquid electrolyte at this low potential, the solvents as well as the salt will start to degrade at ~ 0.8 V for graphite anode and form a passivation layer, which is commonly referred as the solid electrolyte interphase (SEI).[41,42] Although the formation of SEI consumes lithium inventory and leads to irreversible capacity loss, this layer can prevent further severe electrolyte decomposition and ensure the reversibility of the batteries. Spinel structured $Li_4Ti_5O_{12}$, which has a theoretical capacity of 175 mAh/g with ~ 1.5 V working potential, becomes particularly attracting due to the high working potential above 1 V, which is higher than conventional SEI formation potential.[43,44] This could significantly limit the SEI formation and the initial irreversible capacity loss. However, severe gassing during cycling, which causes serious swelling of the batteries, is observed for $Li_4Ti_5O_{12}$ anode, especially at elevated temperature.[45-47]

1.2.2.2 Alloying materials

Alloying reactions of lithium with several metals and semi metals in non-aqueous electrolyte was firstly reported by Dey.[48] Various alloying materials, such as pure Si, Sn, Sb, Al, Mg and their alloys, have been extensively studied afterwards as candidates for the next generation anode materials in lithium-ion batteries due to their higher capacity compared to graphite.[49-51] The alloying reaction is illustrated as the following *Eqn.1*:

$$M + xLi^+ + xe^- \rightarrow Li_XM \qquad Eqn.1$$

Table 1. Characteristics of graphite and alloying materials with various elements as anodes in lithium-ion batteries (Adapted from ref[49])

Material	Fully lithiated phase	Capacity (mAh/g)	Average voltage (V)	Stack energy in full cell (Wh/L)[a]
Graphite	LiC_6	350	0.125	726
Si	$Li_{3.75}Si$	3579	0.400	976
Sn	$Li_{4.4}Sn$	998	0.504	941
Sb	Li_3Sb	660	0.948	796
Al	LiAl	993	0.38	911
Mg	$Li_{1.95}Mg$	2150	0.0325	1032
Zn	LiZn	410	0.310	937

[a]Stack energy in full cell is estimated using the 18650 cell model. Detailed description can be found in ref[49].

Among all these materials, silicon-based materials are considered as the most promising candidates due to their outstanding energy density, affordable cost and moderate operating voltage as presented in *Table 1*. The thermodynamics and kinetics of Li-Si alloying system was firstly studied in the 1970s at elevated temperature (~ 400 °C) and the formation of several different crystalline phases was reported.[52,53] The fully lithiated phase observed in the studies was $Li_{22}Si_5$, which corresponds to a theoretical capacity of ~ 4200 mAh/g. However, the lithiation of silicon was observed to be different

at room temperature by Wilson and Dahn in the study of the electrochemical behavior of graphite with nano-dispersed silicon at room temperature.[54] The crystalline silicon electrode was reported to undergo electrochemically-driven solid state amorphization during first lithiation process by Limthongkul *et al*.[55] Obrovac and Christensen identified the $Li_{15}Si_4$ phase, which corresponds to a theoretical capacity of 3579 mAh/g, as the most Li-rich lithium silicide phase at room temperature.[56] The widely accepted lithiation and delithiation mechanism of micro-sized bulk crystalline silicon anode was later proposed by Obrovac and Krause:[57] during the first lithiation, the crystalline Si undergoes a two-phase reaction which leads to the formation of the amorphous lithium silicide and continued lithiation results in the fully lithiated crystalline $Li_{15}Si_4$ phase. During the following delithiation (charge) process, the $Li_{15}Si_4$ phase transforms back to amorphous Li_xSi.

Although the alloying mechanism of bulk silicon (micro-sized) has been well understood, the electrochemical performance of the electrode is rather limited.[57-59] This is partially due to the particle pulverization caused by significant volume expansion (~280% upon full lithiation to $Li_{15}Si_4$ phase) during lithiation.[56] Reducing the particle down to nano-size has been explored as an effective approach to counter the facture problem[59-62], and has been convincingly confirmed by several in-situ TEM studies on silicon nanoparticles and nanowires.[63-65]

The large volume change of silicon particles during cycling also results in breaking-down of the electrical contact between silicon particles, current collector as well as the conducting additive.[58,66] Moreover, the SEI layer formed on the silicon electrode is unstable and cannot sufficiently prevent continuous electrolyte decomposition.[66] Both of these issues elucidate the importance of the binder to the electrochemical performance of silicon electrodes. Indeed, the conventionally used polyvinylidene fluoride (PVdF) has been proved not suitable for silicon-based materials due to poor adhesion and cyclability.[60,67] Various kinds of binders, especially water-based ones, have been widely explored in recent years and carboxymethyl cellulose (CMC),[67-69] poly(acrylic acid) (PAA)[70,71] and alginate[72,73] are, so far, the most promising candidates. It is believed that the carboxylate group in these binders can be chemically bonded to the native surface of silicon particles which consists of silicon oxide and silanol, and this can significantly improve the electrode adhesion and thus the cycling performance.[49,68,72] In addition, *Mazouzi et al.* demonstrated that using an aqueous solution which was buffered to pH 3 during the slurry preparation can further promote the bonding between Si particles and CMC binder.[74,75]

The SEI formed on silicon-based anodes in conventional $LiPF_6$ based liquid electrolyte lithium-ion batteries has been studied and is found to mainly consist of LiF, lithium alkoxide, carbonates such as lithium alkyl carbonates, Li_2CO_3 as well as polycarbonates.[76-79] Moreover, it has also been observed using photoelectron spectroscopy (PES) that the native oxide surface on

silicon particles will be affected upon cycling and storage with $LiPF_6$-based electrolytes and form new species as SiO_xF_y, Li_xSiO_y.[77,80] An alternative salt, lithium bis(fluorosulfonyl)imide (LiFSI), has been examined and shows better compatibility with nano-silicon electrode due to better stability towards the silicon surface.[81] Introducing additives to the conventional liquid electrolyte is also a promising approach to improve the SEI stability and cyclability of the silicon anode. Among all the explored additives, fluoroethylene carbonate (FEC) and vinylene carbonate (VC) are found to be the most effective two to improve capacity retention and coulombic efficiency.[82-84] Surface coating on silicon, such as carbon,[85-88] TiS_2,[89] conductive polymer polypyrrole[90] and poly(3,4-ethylenedioxythiophene),[91] etc., is another approach to improve the interfacial stability as well as enhance electrical conductivity.

Although the performance has been dramatically improved, silicon-based alloy electrodes have not been widely commercialized so far, as graphite is still the dominating anode material. Besides some of the intrinsic limitations described in previous paragraphs, several practical aspects, such as high price of producing high-purity nano-silicon, high cost and safety risk of battery manufacturing with nano-sized powders, difficulty in producing high quality electrode coating at industry-scale,[75,92] etc., have to be addressed before large-scale application of nano-silicon electrodes. Obrovac and Chevrier also highlighted the importance of coating design for alloy anode materials in order to achieve energy density improvement from conventional graphite electrodes.[49] Nevertheless, in 2005 Sony has commercialized a Sn-Co-C alloy anode in the ‘‘Nexelion’’ cell and a 10% improvement in terms of energy density in full cell model (LCO cathode) compared to standard graphite electrode.[49]

1.2.2.3 Conversion materials

The other class of anode materials is referred to conversion materials, and it is usually a transition metal coupled with an anion. The electrochemical reaction, which conversion materials typically undergo, is illustrated as *Eqn. 2*:

$$M_xN + yLi^+ + ye^- \leftrightarrow xM + Li_yN \qquad Eqn.2$$

where M = transition metal (e.g. Fe, Co, Mn, etc.) and N = anion (e.g. O, S, P, etc.). The most studied conversion-type anode materials are metal oxides, e.g. α-Fe_2O_3,[93,94] Fe_3O_4,[95,96] MnO_2,[97,98] etc., which have several advantages such as high theoretical capacity and low cost. However, most of the transition metal oxides suffer from high voltage hysteresis (voltage difference between change and discharge), which results in low energy efficiency. This is due to the slow kinetics of the conversion reaction.[99] Besides, issues, such as volume changing during cycling, unstable SEI and poor capacity retention, are still limiting large-scale application of these materials.

1.3 Electrolyte

The electrolyte, which is the Li^+ transporting media during cycling, is another key component in lithium-ion batteries. The electrolyte applied in lithium-ion batteries consists of a lithium salt and its hosting material, and so far several different electrolyte systems have been developed, such as liquid electrolyte,[100] gel electrolyte,[101] ceramic electrolyte,[102] solid polymer electrolyte[103] and ionic liquid.[104] Among all these, small-molecule carbonates based non-aqueous liquid electrolyte has been most widely used mainly due to its superior Li^+ ion conductivity at room temperature, for example, $LiPF_6$ salt in ethylene carbonate (EC) and diethyl carbonate (DEC).

Although questioned about its chemical and thermal stability, $LiPF_6$ remains as the most commonly used lithium salt in today's commercial lithium ion-batteries.[105] It is believed that any remaining moisture in the battery will hydrolyze $LiPF_6$, and one of the reaction products HF is highly corrosive towards electrode materials.[106] Various new lithium salts have been developed in to order to achieve better battery performance, such as lithium borates (e.g. lithium difluorooxalatoborate (LiDFOB),[107,108] dilithium dodecafluorododecaborate (Li2DFB)[109]), imides (e.g. lithium bis(fluorosulfonyl)imide (LiFSI),[110] lithium 4,5-dicyano-2-trifluoromethanoimidazole (LiTDI)[111,112]). The solvents used in the liquid electrolyte are also essential and most commonly, mixed solvents are applied to achieve both high dielectric permittivity (EC) and low viscosity (e.g. dimethyl carbonate (DMC), DEC, ethylmethyl carbonate (EMC)).[100,105] These carbonate solvents as well as the salts are not electrochemically stable at the operation voltages of lithium-ion batteries and will be decomposed at the electrode/electrolyte interface. In order to obtain good battery cycling performance and safety, small amounts of chemical components are usually added to the electrolyte and referred as electrolyte additives. Depending on the different functionalities, some of the most commonly used additives are summarized in Table 2.

Table 2. *A brief summary of different types of electrolyte additives with examples.*

Types	***Examples***
Additives for anode	LiDFOB,[113] VC,[114,115] FEC[84,116,117]
Additives for cathode	LiBOB,[118,119] LiDFOB, [120,121]
Additives for overcharge protection	Ferrocene,[122] phenothiazines,[123] 1,3,2-benzodioxaborole[109]
Flame retardant additives	Trimethyl phosphate,[124] triphenyl phosphate[125]

In general, additives for anodes and cathodes are used to improve the electrode/electrolyte interfacial stability. Redox shuttle chemicals, which interact with both electrodes but do not become part of their interphases, are usually employed as additives for overcharge protection. Introducing flame

retardant additive can decrease the flammability of the liquid electrolyte, and thus enhance battery safety.

1.4 Electrode/electrolyte interface

The high output voltage of lithium-ion batteries requires a wide electrochemical stability window of the electrolyte in order to match the operation potential of the two electrodes.[100,105] Ideally, the potential window should be larger than the operating potential difference between cathode and anode, i.e. the output cell voltage as shown in *Figure 2(a)*, so that there will be no side reactions occurring at the electrode/electrolyte interfaces. However, the conventionally used carbonate-based solvents are not thermodynamically stable in this potential window. LFP//graphite battery chemistry is demonstrated as an example in *Figure 2(b)*. The potential of LFP is within the electrolyte stability range while the anode side, i.e. graphite, is beyond. This results in reduction of the electrolyte at the graphite surface, and formation of a passive SEI layer, which prevents further continuous electrolyte degradation. The formation of SEI on graphite electrodes is usually found at potential around 0.8 V vs. Li/Li^+ and thus mainly occur before the first lithiation of graphite.[42,126,127] Besides, a few cathode materials operate at potentials higher than the stable limit of carbonate-based electrolyte (4.5 V), such as spinel LNMO (4.6 V), LiCoPO4 (4.8 V), and therefore will require electrolyte additives or alternative solvents.

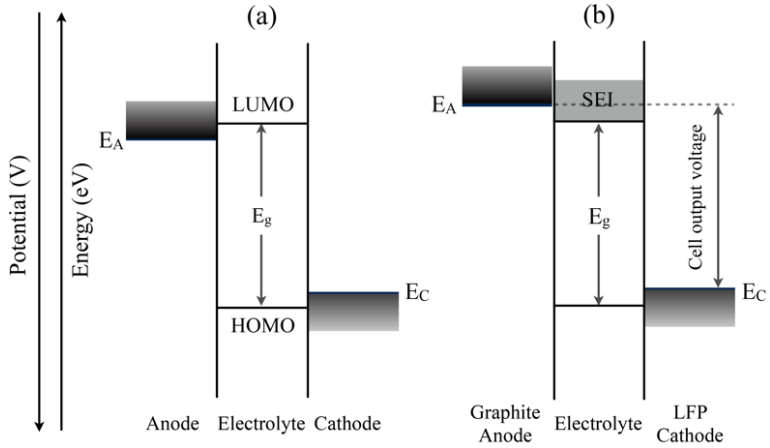

Figure 2. A schematic illustration of the SEI formation in an LFP//Graphite battery.

The nature of the SEI has been extensively explored but still it has not been fully understood due to its complexity as well as the difficulty in characterization since the thickness of the SEI layer is usually only a few Å to several nanometers.[42,127] Moreover, the SEI is also sensitive to air exposure and requires an air-free environment for the sample preparation, transfer as

well as measurement.[128] As a result, surface sensitive techniques, such as X-ray photoelectron spectroscopy (XPS),[80,129,130] atomic force microscopy (AFM),[114,130,131] time of flight-secondary ion mass spectroscopy (TOF-SIMS),[132,133] have been most frequently used. Scanning electron microscopy (SEM), Transmission electron microscopy (TEM), Fourier transform infrared spectroscopy (FT-IR), Raman spectroscopy, etc., are also widely applied to obtain more information of the SEI layer.[78,134,135]

Nevertheless, the fact that the SEI usually contains both organic and inorganic species, which are degradation products of the salt and solvents in the electrolyte, has been widely accepted.[42,127] Possible degradation mechanisms of some commonly used the lithium salt as well as the electrolyte solvents, such as $LiPF_6$, EC, DEC, DMC, PC, have been proposed and illustrated in *Scheme. 1*.[134] Li_2CO_3, lithium alkyl carbonates, lithium alkoxides, poly(ethylene oxide), polycarbonates and LiF are commonly found as SEI components from the decomposition of the electrolyte.

Scheme. 1 Possible degradation mechanisms of some commonly used electrolyte salt and solvents.

$$EC + 2e^- + 2\,Li^+ \rightarrow Li_2CO_3 + CH_2{=}CH_2$$

$$2EC + 2e^- + 2\,Li^+ \rightarrow (CH_2OCO_2Li)_2 + CH_2{=}CH_2$$

$$DMC + e^- + Li^+ \rightarrow CH_2OLi + CH_2OCO\bullet + CH_2OCO_2Li + CH_2\bullet$$

$$R\bullet + Li^+ + e^- \rightarrow RLi$$

$$nR\bullet \rightarrow R_n\ (polymer)$$

$$2ROCO_2Li + H_2O \rightarrow Li_2CO_3 + 2LiOH + CO_2$$

$$LiPF_6 \leftrightharpoons LiF + PF_5$$

$$PF_5 + H_2O \rightarrow PF_3O + 2HF$$

$$ROCO_2Li + HF \rightarrow ROCO_2H + LiF$$

$$ROLi + HF \rightarrow ROH + LiF$$

The formed passive SEI layer can significantly influence the electrochemical performance of the batteries. Ideally, the SEI should be electronically insulating to prevent further electrolyte reduction, and at the same time ionically conductive to allow Li^+ transporting upon cycling.[127] The layer should be uniform, stable and flexible to protect the electrode and accommodate volume change of the electrode during the cycling. Although the formation of the SEI is beneficial for the batteries in terms of preventing continuous electrolyte degradation, most of the SEI components contain Li^+ and its formation will consume the Li-inventory in the battery system, resulting in irreversible capacity loss. Moreover, this passive layer also strongly affects the battery performance such as capacity retention, rate capability, etc.

2. Scope of this thesis

The aim of the Ph.D project is to develop a novel battery chemistry using lithium metal silicate as the cathode and silicon as the anode, both of which are based on the earth-abundant element Si. This enables the possibility of reducing the cost of the electrode materials. Li_2FeSiO_4 has the potential of extracting two Li^+ per molecular formal and giving high energy density. The silicon anode also has a significant advantage of high specific energy over the conventionally used graphite.

This thesis work has been mainly focused on improving the performance of the silicon anode and understanding the interfacial chemistry of the silicon electrode where the unstable SEI is limiting the long-term performance. Therefore, the surface-sensitive technique PES has been applied as the main characterization tools to study the SEI on silicon electrodes. The combination of conventional in-house XPS and synchrotron radiation based PES enables a unique non-destructive depth profiling of the SEI. Besides, improving the battery performance via exploring electrode formulation, electrolyte composition and cycling conditions is another important aspect of this work.

3. Method

3.1 Battery preparation

Conventional silicon electrodes (used in paper **I** and **II**) were prepared by casting a slurry onto a copper foil using doctor-blading technique. The electrode slurry was a mixture of silicon nanoparticles (SiNPs, average partical size ~50 nm, Alfa Aesar), carbon black (Super P, Erachem Comilog), and sodium carboxymethyl cellulose (CMC-Na, DS = 0.9, Mw = 700000, Sigma-Aldrich) (80:12:8, mass ratio). The solid components were ball milled for one hour in a water-ethanol solution (70/30, v/v). Circular electrodes (average mass loading of 1.65 mg per electrode) with a diameter of 20 mm were punched out after 12 h pre-drying at 60 °C and the electrodes were further dried at 120 °C for 12 h inside an argon-filled glovebox (O_2 < 2 ppm, H_2O < 1 ppm).

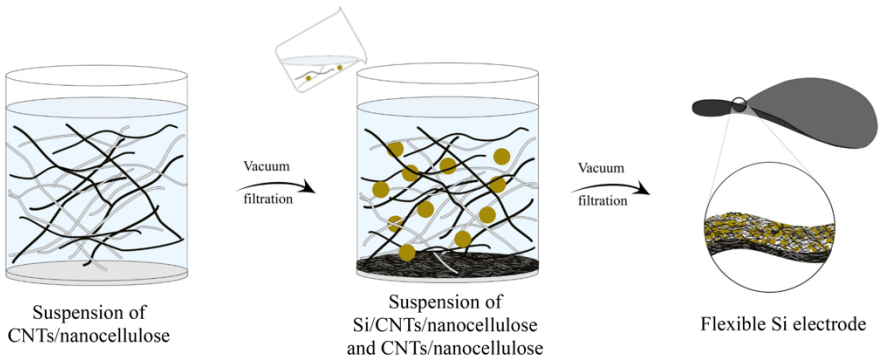

Figure 3. A schematic representation of the preparation processes of the freestanding silicon electrode. Reprinted with permission from ref[136]

Freestanding silicon paper electrodes (used in **paper III**) were prepared by two-steps vacuum filtration as shown in *Figure 3*: firstly, 20 mg *Cladophora* nanocellulose (CNC) and 20 mg carboxylic acid functionalized multi-walled carbon nanotubes (CNT) were dispersed in 60 mL water by sonication (Sonics and Materials Inc., USA, Vibra-Cell 750). The obtained dispersion was vacuum filtered through a nylon membrane filter (0.45 μm); and secondly, another 50 mL dispersion consisting of 30 mg SiNPs, 20 mg CNC and 30 mg CNT was poured onto the CNT/CNC substrate layer, and the SiNP/CNT/CNC paper electrode was obtained via another vacuum filtration.

The SiNP/CNT/CNC paper electrode consisted of the SiNP, CNC and CNT in the mass ratio of 25%, 33% and 42%, respectively. The freestanding electrode was ~30 μm in thickness and the Si mass loading was 0.78 mg/cm^2.

Three different electrolytes used in this thesis are listed in Table 3. The LP40 electrolyte was produced by Merck and used as received. The FEC/LP40 electrolyte was prepared by mixing 90 wt% LP40 and 10 wt% FEC (99%, Aldrich). The LiTDI was dried at 170 °C for 12 h prior to electrolyte preparation.

Table 3. *List of the electrolytes used in this thesis*

Electrolytes	
1 M $LiPF_6$, EC/DEC = 1/1, Merck (LP40)	**Paper I**
90% LP40, 10% FEC (FEC/LP40)	**Paper I, III**
0.6 M LiTDI, EC:DMC = 1:2	**Paper II**

The batteries were assembled by sandwiching two layers of electrolyte-soaked Solupor separators between the silicon electrode and lithium foil (CYPRUS Foote Mineral Co.), and vacuum-sealing the stacks as pouch-cells in the glovebox.

3.2 Characterization techniques

In this thesis work, galvanostatic cycling and photoelectron spectroscopy have been used as the main characterization techniques, and will be introduced in detail in the following sections. Besides, SEM (SEM/EDS Zeiss 1550), FT-IR (Spectrum One FTIR spectrometer, equipped with a Diamond/ZnSe crystal (PerkinElmer, U.S.)) and Raman (Renishaw Ramascope) were also used.

3.2.1 Electrochemical characterizations

Galvanostatic cycling has been used to evaluate the electrochemical performance of all the batteries in **paper I, II and III**. During a galvanostatic experiment, a constant current is applied to the battery and the response of the battery voltage is monitored as a function of time. The applied current is calculated with the chosen C-rate (C/5, 1C and 5C correspond to full charge or discharge in 5 hours, 1 hour and 12 min respectively). Different cut-off conditions (voltage, time, etc.) can be used, and in **paper I, II and III,** constant cut-off voltages are applied. A rate capability test has been performed in **paper III** and it was carried out by galvanostatically cycling the battery at different current densities. The coulombic efficiency for silicon half cells is calculated with *Eqn. 3*:

$$Coulombic\ efficiency = \frac{C_{charge(delithiation)}}{C_{discharge(lithiation)}} \times 100\% \qquad Eqn.3$$

Two additional electrochemical techniques, cyclic voltammetry (CV) and electrochemical impedance spectroscopy (EIS), are also used in **paper I**. In a cyclic voltammetry experiment, the potential of the working electrode is linearly scanned and the current is examined as a function of the potential. The peak current and peak potential in the obtained cyclic voltammogram can be used to evaluate the reaction thermodynamics, kinetics, etc. EIS is a technique to measures the impedance of a battery over a range of frequencies. The magnitude of the applied ac voltage is usually rather small (e.g. 10 mV).

3.2.2 Photoelectron spectroscopy

Photoelectron spectroscopy (PES) is a surface sensitive characterization technique that provides information of the elemental composition, chemical and electronic states of the elements within a material. Therefore, PES has been one of the most widely used techniques to investigate the composition of the SEI in lithium-ion batteries, and it is applied as the main characterization technique in **paper I** and **II**.

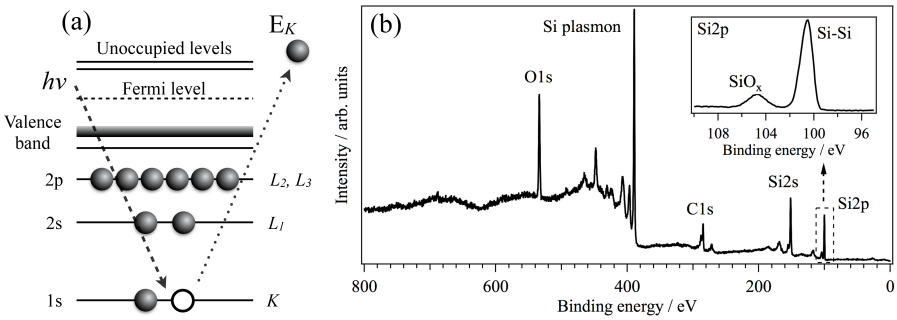

Figure 4. (a) A schematic presentation of the working principle of the PES and (b) a overview spectrum of a pristine silicon composite electrode.

The working principle of the PES technique is based on the photoelectric effect and a schematic illustration is shown in *Figure 4(a)*. During the measurement, the sample is irradiated with photons with a specific energy (hv) and emits photoelectrons after excitation. The kinetic energy of the photoelectrons is examined by an electron analyzer. The binding energy of photoelectron (E_B) can be calculated with *Eqn. 4*:

$$E_B = h\upsilon - E_K - \phi \qquad Eqn.4$$

where E_K is the kinetic energy of the emitted photoelectrons and ϕ is the work function dependent both on the spectrometry and the sample. As the

binding energies of the photoelectrons from specific atomic core levels are rather defined, the PES technique is able to identify the elemental composition at the surface of the sample. As an example, the overview spectrum of a pristine silicon composite electrode is demonstrated as *Figure 4(b)*, which shows the presence of C, O and Si on the sample. Moreover, the binding energy of the same element can be varied depending on the specific chemical states, known as the ''chemical shift''. In the *Figure 4(b)*, the Si 2p spectrum shows that it consists of contributions from the elemental Si (Si-Si) and the native oxide species (SiO_x).

For a conventional PES measurement on a flat sample, the intensity of a core level signal can be described as *Eqn. 5*:

$$I \propto I_0(\sigma \cdot \rho \cdot S) \cdot exp\left(\frac{-d}{\lambda sin\theta}\right) \qquad Eqn.5$$

where I is the intensity of the detected photoelectrons, I_0 is the intensity of emitted photoelectrons, σ is the cross section, ρ is the surface concentration of the element, S is the analyzer transmission of the photoelectrons, $d/sin\theta$ is the travel distance of the photoelectrons and λ is the electron inelastic mean free path (IMFP). The cross section is specific for each core levels but will be varied at different excitation energies (usually decreases as the excitation energy increases). The IMFP describes how far an electron can travel in a solid before loosing energy. It is dependent on the kinetic energy of the electrons, and for a PES experiment, the IMFP can be varied by changing the excitation energy. In this work, the probing depth of PES is referred to 3λ, as this includes 95 % of the total elastically emitted photoelectrons. In order to achieve non-destructive depth profiling, PES measurements have been carried out with different excitation energies with three set-ups (listed in *Table 4*) in this thesis work. The most surface-sensitive measurements are carried out at the I411 beamline at MAX-lab with low photon energy. At the KMC-1 beamline, BESSY, it is possible to probe the bulk part of the sample since the excitation energy is available up to 12 keV.

Table 4. *A summary of the three PES setups used in this thesis work.*

Setup	**Excitation energy**
Beamline I411 at MAX-lab, Lund, Sweden	50 – 1500 eV
In-house ESCA	AlKα (1487 eV)
Beamline KMC-1 at BESSY, Berlin, Germany	2000 – 12000 eV

For all the PES measurements, the samples were washed with DMC three times before transferring to the spectrometer in order to remove the electrolyte residue. Air-tight transfer chambers were used for all the sample transfer to avoid are-exposure, which can significantly influence the results in studying the SEI as demonstrated by previous studies.[128] The obtained spectra were curve fitted with Gaussian-dominated (< 10 % Lorentzian) peak shape

using Igor Pro software and the spectra were calibrated versus the hydrocarbon (C-C/C-H) C 1s peak at 285 eV.

4. Improving the performance of silicon based anode materials

4.1 FEC as electrolyte additive

This chapter describes the FEC electrolyte additive for silicon based electrode in lithium-ion batteries. The aim was to study how the FEC affects the electrochemistry and the SEI on the silicon electrodes. Results presented in this chapter are based on **Paper I**.

4.1.1 Electrochemical results

Silicon half-cells with two different electrolytes LP40 and FEC/LP40 (10 wt% FEC and 90 wt% LP40), respectively, have been investigated with cyclic voltammetry and galvanic cycling in order to investigate the influence of the FEC additive and the results are presented in *Figure 5*.

In the cyclic voltammetry results shown in *Figure 5(a),* a unique reduction peak at potential ~1.3 V is visible only for FEC/LP40, indicating that this peak corresponds to the reduction of FEC. With a higher reduction potential than the conventional SEI formation (~0.8 V) from electrolyte decomposition, FEC is reduced prior to the other solvents and thus quickly forms a surface layer, which mainly consists of its degradation products. Furthermore, long-time cycling performance was substantially improved with the 10% FEC additive as presented in *Figure 5(b)*. It should be noted here that 4 pre-cycling steps (details are included in **paper I**) have been applied to both of the batteries prior to the long-term cycling. Only 5 % capacity (referring to 1200 mAh/g) is lost after 80 cycles with FEC additive whereas as high as ~30% loss is observed without FEC. The coulombic efficiency is constantly retained at ~99% over the 85 cycles for FEC/LP40 battery but continuously decreased to ~97 % for LP40 battery. The potential profile of 1^{st}, 10^{th} and 85^{th} cycle are shown in *Figure 5(c)* and *(d)* for the silicon half-cells cycled with or without FEC, respectively. The decrease in the lithiation potential is found significantly less for the FEC/LP40 sample after 85 cycles compared to the LP40 sample, and this results in less capacity fading as constant potential cut-offs were used.

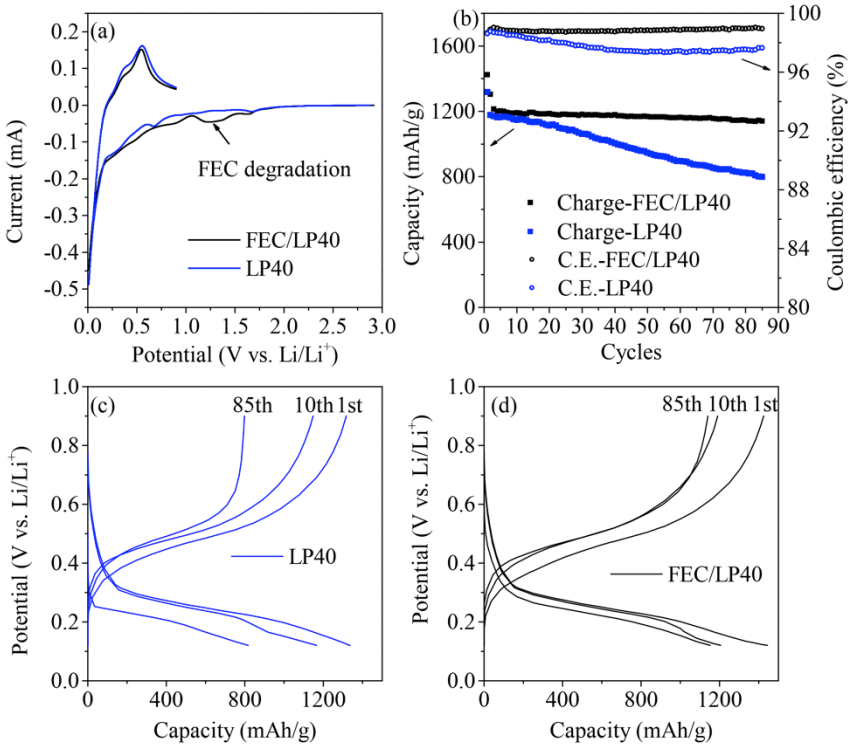

Figure 5. (a) Cyclic voltammogram of the first electrochemical cycle of silicon half-cells with FEC/LP40 (black) and LP40 (blue) electrolyte, respectively. (b) Gravimetric capacities and coulombic efficiencies of the silicon half-cells between 0.12 V and 0.9 V at 500 mA/g (Si) using FEC/LP40 and LP40 electrolytes, respectively. (c and d) Discharge and charge potential profile at 1st, 10th, and 85th cycles for the LP40 and FEC/LP40 cells, respectively.

4.1.2 Surface morphology

The surface morphology of the pristine silicon electrode (*Figure 6a, b*), and the electrodes after 85 cycles with electrolyte LP40 (*Figure 6c, d*) and FEC/LP40 (*Figure 6e, f*), respectively, are presented in *Figure 6*. A large number of cracks were formed on the electrode cycled with LP40 while the FEC/LP40 cycled electrode surface was retained smooth as pristine, as shown in the low magnification images. Moreover, for the LP40 sample, the surface of the silicon particles is unevenly covered by the SEI, which also severely blocks the surface voids and limits the access of the electrolyte. These effects would all cause the observed increase in polarization and fast capacity fading. By adding 10 wt% FEC into the LP40 electrolyte, the surface morphology can be well preserved over long-time cycling due to the conformal and stable SEI formed. Overall, these results demonstrate the

essential importance of the morphology and stability of the SEI layer for the battery performance.

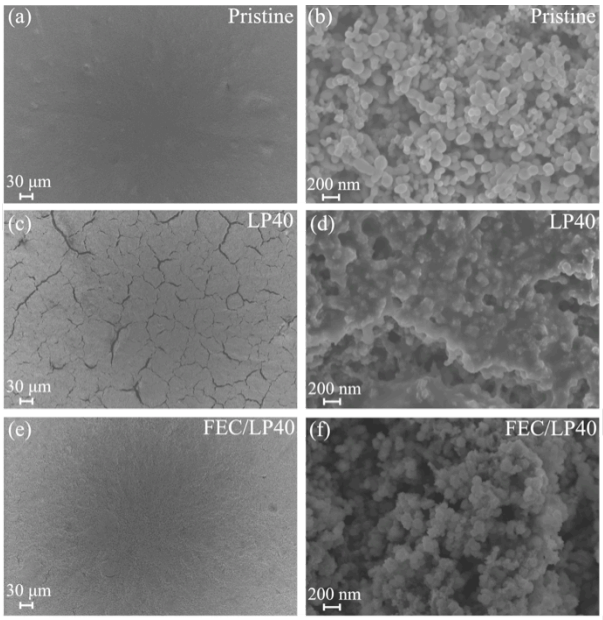

Figure 6. Surface morphologies of the pristine silicon electrode (a,b), after 85 cycles with the LP40 electrolyte (c,d), and FEC/LP40 electrolyte (e,f). Reprinted with permission from ref[137].

4.1.3 Photoelectron spectroscopy results

Synchrotron radiation based photoelectron spectroscopy with various photon energies was utilized to trace the FEC decomposition mechanism as well as the difference in the SEI compositions between the FEC/LP40 and LP40 battery in **paper I**. All the PES samples were washed with DMC prior to the measurements to remove electrolyte residues (details described in **paper I**).

4.1.3.1 FEC decomposition reaction

As the cyclic voltammetry results in *Figure 5* indicate, the reduction of FEC occurs at ~1.3 V. Constant current was applied to a silicon half-cell and the battery was discharged to 0.9 V before disassembly, to study FEC decomposition reaction. The comparison between OCV sample (open circuit voltage, soaked in electrolyte) and 0.9 V sample is presented in *Figure 7*, including the F 1s, O 1s and C 1s spectra. Selected photon energies were used for each core levels, i.e. 835 eV for F 1s, 680 eV for O 1s and 430 eV for C 1s, in order to achieve the same kinetic energy of ~140 eV for the photoelectrons, hence the same probing depth. This low kinetic energy leads to a probing

depth of ~2 nm, which is extremely surface sensitive and suitable for evaluating the FEC decomposition products.

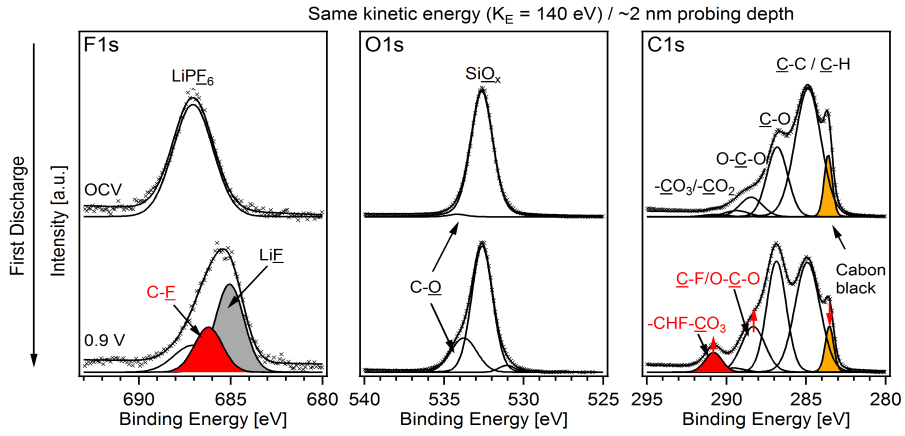

Figure 7. F 1s, O 1s and C 1s spectra of the silicon electrode at OCV and 0.9 V (during first discharge). The electrolyte used was FEC/LP40. The spectra were recorded with the same kinetic energy of 140 eV for all the core levels studied.

Scheme. 2 Possible FEC decomposition reactions and products. Reprinted with permission from ref[137].

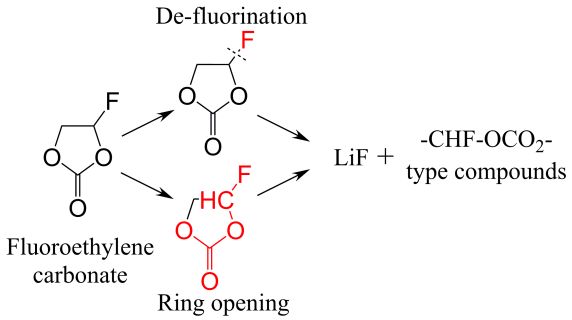

No FEC residue was observed on the OCV sample after washing since the F1s, O1s, C1s spectra for the OCV sample are dominated by the pristine materials $LiPF_6$, SiO_x, CMC-Na and carbon black. Once the reduction of FEC occurred as the batteries were discharged to 0.9 V, LiF, which is a commonly observed SEI component in F-containing batteries, was formed as one of the decomposition compounds and detected on the silicon electrode surface (0.9 V sample). Both the de-fluorination of FEC and $LiPF_6$ can contribute to the formation of LiF. Besides, a new C 1s features at binding energy ~290.8 eV (C 1s peak with red filling in *Figure 7*) emerged for the 0.9 V sample compared to the OCV sample. The signal corresponds to –CHF-OCO_2- type compounds since the binding energy observed is slightly higher than conventional carbonate species (usually at ~290 eV) and this increase is

attributed to the presence of –CHF- group. The C-F (686 eV in F 1s) and C-O (533.7 eV in O 1s) features further confirm the interpretation. And based on the identified species, two possible FEC decomposition reactions on silicon electrodes are proposed in **paper I** and illustrated in *Scheme. 2*. Firstly, FEC undergoes de-fluorination and forms LiF as one of the main degradation products. Secondly, the five-membered ring opens, followed by reactions, e.g. polymerization, and generates –CHF-OCO_2- type compounds.

4.1.3.2 SEI composition after long cycling and salt decomposition

The SEI after long-term cycling (current density 500 mA/g of Si, 85 cycles) with FEC/LP40 and LP40 electrolyte, respectively, has also been studied with PES characterization. Surface atomic contractions of these two samples were calculated from in-house XPS measurements (AlKα, hν = 1487 eV) and the results are listed as *Table 5*.

Table 5. *Surface atomic concentration of silicon electrode after 85 cycles with FEC/LP40 and LP40 electrolytes, respectively.*

Electrolyte	***F 1s (%)***	***O 1s (%)***	***C 1s (%)***	***P 2p (%)***	***Si 2p (%)***	***Li 1s (%)***
FEC/LP40	15.7	26.4	36.6	0.5	0.3	20.5
LP40	4.1	31.9	48.7	0.9	0.4	14.0

Overall, the atomic concentration is significantly different between the electrodes cycled with FEC/LP40 and LP40 electrolyte. Much more fluorinated species were found on the FEC/LP40 sample (15.7%) compared to LP40 sample (4.1%). De-convolution on high-resolution F 1s spectra in **paper I** shows that the main F-containing compound on the silicon electrode cycled with FEC/LP40 sample is LiF. The SEI on LP40 sample is more dominated carbon and oxygen containing compounds. C 1s spectra, one of the most important core levels for SEI investigation, measured at different photon energies of 430 eV, 2005 eV, and 6015 eV are presented in *Figure 8* for the two different kinds of batteries. The signal at ~290.8 eV (highlighted with red filling), which corresponds –CHF-OCO_2- type compounds as FEC decomposition products, can be observed for all FEC/LP40 C 1s results. However, none of the LP40 results has the presence of such signal, and this confirms that this feature is attributed to the derivatives of FEC. Instead, the peak at highest binding energy for LP40 samples is located at 290 eV, corresponding to conventional carbonated species generated from the degradation of the solvents, i.e. EC and DEC. Moreover, the C 1s signals for O-C-O and –OCO_2- type compounds are slightly different between the two systems, indicating different chemical compositions. This is, most likely, because of the degraded FEC segments are taking part in the formation of such compounds.

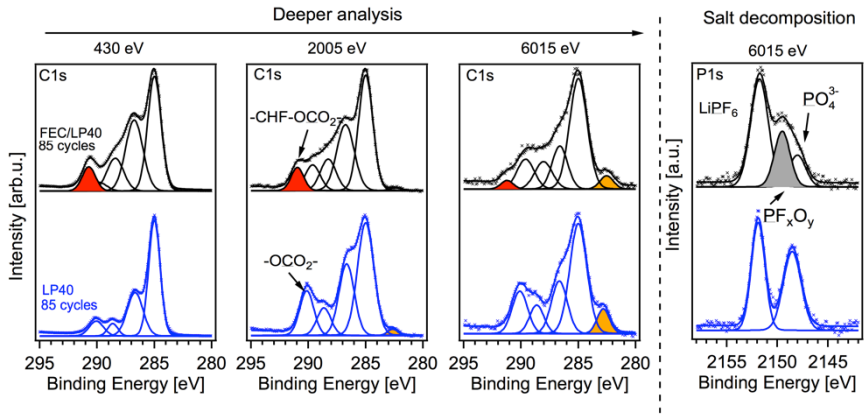

Figure 8. C 1s (hν = 430 eV, 2005 eV and 6015 eV) and P 1s (hν = 6015 eV) spectra of the silicon electrodes after 85 cycles with FEC/LP40 and LP40 electrolytes, respectively.

The thermodynamic instability of $LiPF_6$ in this study (**paper I**) is well known and the possible decomposition reactions have been illustrated in *Scheme. 1*. In order to study the potential influence of FEC additive to the degradation of $LiPF_6$, P 1s measurements (hν = 6015 eV) were carried out, and the results for FEC/LP40 and LP40 samples are shown in *Figure 8*, respectively. Indeed, one additional P 1s peak at ~2149.6 eV (highlighted with grey-filling in *Figure 8*) is observed for the FEC/LP40 sample in addition to the two common features (~2152 eV and ~2148.3 eV) for both the samples. This unique peak is attributed to PF_xO_y and the presence of the higher fluorinated phosphoric oxides spices compared to phosphate (~2148.3 eV) indicates the suppression of the deep degradation of $LiPF_6$. It is probably due to the decomposed FEC segments interacting with the salt and forming stable intermediate products. Meanwhile, the stable SEI layer formed with the FEC additive may also prevent further degradation of $LiPF_6$.

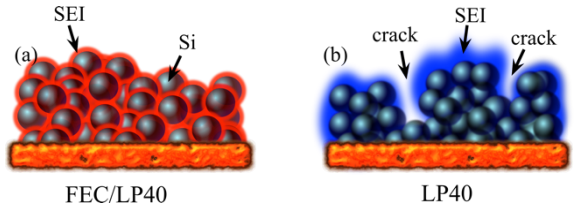

Figure 9. Schematic representation of the SEI formation on a silicon electrode after long-term cycling with eletrolytes FEC/LP40 (a) and LP40 (b), respectively.

Based on the results, the effect of FEC additive on the SEI formed on silicon electrodes has been illustrated as *Figure 9*. FEC as an electrolyte additive degrades prior to other electrolyte solvents, and forms a conformal and

stable SEI. This SEI layer consists of a substantially higher amount of LiF compared to the SEI on the silicon electrode cycled with LP40-only electrolyte. -CHF-OCO_2- type compounds from the decomposition of FEC are also observed on FEC/LP40 sample. The SEI layer with the presence of FEC can sufficiently limit further electrolyte degradation as well as formation of large amounts of cracks in the electrode, which will lead to the increase in polarization and significant capacity fading. The study demonstrates the importance of FEC as an electrolyte additive for silicon-based anode and the insight of the modification mechanism of FEC.

4.2 LiTDI as an alternative lithium salt

The most commonly used lithium salt, $LiPF_6$, is found to be thermodynamically unstable and can significantly affect the surface chemistry of silicon-based electrodes in lithium-ion batteries. In this section (based on **paper II**), LiTDI is studied as an alternative choice of lithium salts for conventional silicon composite electrodes.

4.2.1 Electrochemistry and surface morphology

The first electrochemical cycle was perform at a current density of 150 mA/g with the 0.6 M LiTDI (in EC: DMC = 1: 2) electrolyte and the potential profile is shown as *Figure 10(a)*. Batteries at different states of charge, which have been highlighted with dots, have been further investigated with SEM and PES. During the first cycle, specific capacities of 2700 and 1500 mAh/g were obtain for the lithiation and delithiation processes, respectively, and the irreversible capacity loss was ~1200 mAh/g (44.4 % of the first lithiation capacity). This indicates a large amount of SEI formation during the first cycle and it is supported by the SEM image of the silicon electrode after one cycle (*Figure 10(c)).*

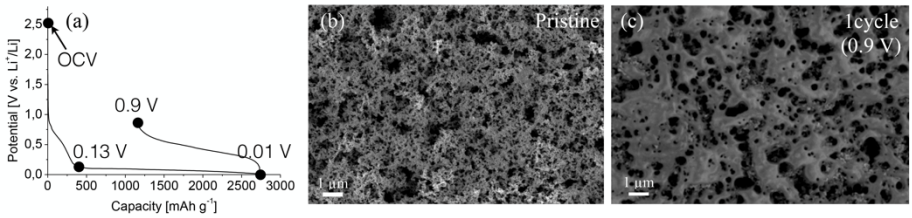

Figure 10. (a) The potential profile of the silicon electrode during the first electrochemical cycle with LiTDI based electrolyte. (b,c) SEM images of the pristine silicon electrode and after the 1st electrochemical cycle, respectively.

4.2.2 Characterization of the SEI

Photoelectron spectroscopy was utilized to study the composition of this SEI layer, and the survey as well as C 1s spectra of OCV (soaked in the electrolyte), 0.01 V (end of lithiation) and 0.9 V (end of deliathiation) samples are shown in *Figure 11*, respectively. Strong O 1s, C 1s and Si signals are dominating the overview spectra of the OCV sample, and the F 1s feature indicates the presence of salt residue on the sample. The other core level from the LiTDI salt, N 1s, cannot be identified since it is overlapping with the strong Si plasmon signals. After the first lithiation and delithiation, a thick SEI was formed as no evident Si signals can be observed from the survey spectra of the 0.01 V and 0.9 V sample, and instead, the spectra mainly consist of F 1s, O 1s, N 1s and C 1s signals. C 1s is one of the most important

core levels for investigating SEI layer and the de-convoluted C 1s spectra for the OCV, 0.01 V and 0.9 V samples are shown in *Figure 11*.

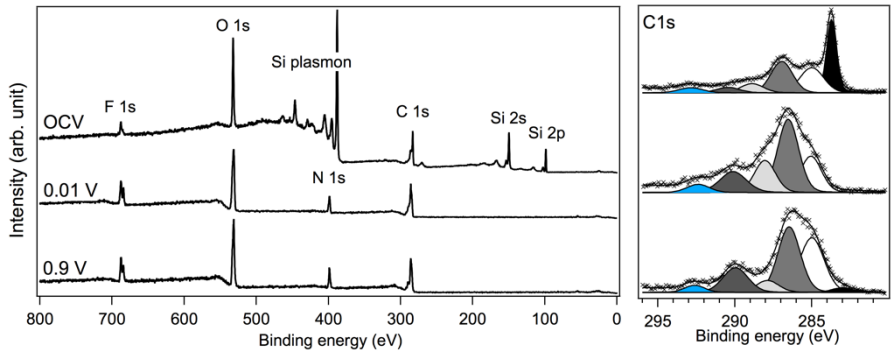

Figure 11. Survey and C1s spectra of the OCV, 0.01 V (end of lithiation) and 0.9 V (end of delithiation) silicon electrode sample. The measurements were performed with a photon energy of 2005 eV.

The C 1s spectrum of the OCV sample reveals the carbon black, CMC-Na as the pristine materials as well as the $–CF_3$ group from the LiTDI. After the first lithiation, the carbon black signal is no longer visible, confirming the formation of a thick SEI layer. The C 1s features of the SEI components are found at 285, ~286.7, ~288 and ~290 eV, corresponding to hydrocarbon (-C-C-/-C-H), -C-O-, -O-C-O- and $-OCO_2-$ type environments, respectively. These are consistent with some of the most commonly found SEI species, e.g. hydrocarbon, ether-type and carbonate species, from the decomposition of the electrolyte solvents. Similar species, but with different relative amounts, were found on the 0.9 V sample.

4.2.3 The silicon surface chemistry and salt decomposition

Philippe, et al. revealed that the pristine silicon oxide surface layer on the silicon particles can be significantly affected by soaking and electrochemical cycling with $LiPF_6$-based electrolyte.[80,81] In order to verify the potential influence from the LiTDI-based electrolyte, Si 1s were investigated and the results of the pristine, OCV, 0.13 V, 0.01 V and 0.9 V samples are shown in *Figure 12*. The same two features, which are bulk Si (~1839 eV) and SiO_2 (~1844 eV) were observed on both the pristine and the electrolyte soaked OCV sample. After initial SEI formation, both the two Si 1s signals are slightly shifted to lower binding energy and there might be two possible reasons for this behavior. Firstly, the surface oxides could be lithiated during this electrochemical process and the changed chemical environment contributed to the shift in binding energy. Secondly, the work function and the Fermi level of the sample could be changed after the formation of the SEI. Simi-

lar observation on graphite electrode has also been reported.[138] The binding energy of the bulk Si/Li_xSi signal is significantly lowered to ~1836 eV after the first lithiation and this is mainly attributed to the change in chemical composition, i.e. lithiation of silicon. As the lithium being extracted during delithiation, this peak shifts back to ~1837.5 eV. Overall, no new Si 1s feature appears after the first electrochemical cycle with the LiTDI-based electrolyte.

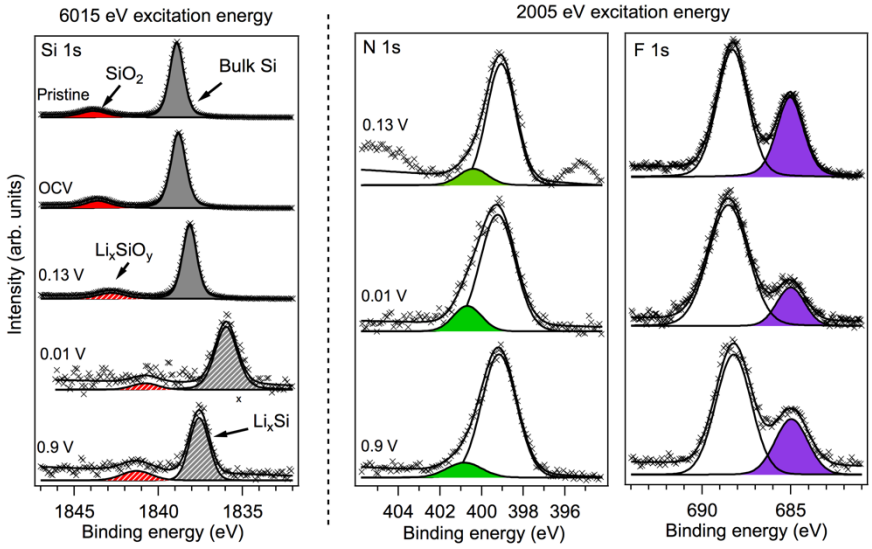

Figure 12. Si 1s spectra of the pristine, OCV, 0.13 V, 0.01 V and 0.9 V silicon electrode sample, and the measurements were carried out with an excitation energy of 6015 eV. N 1s and F 1s (2005 eV excitation energy) spectra of the 0.13 V, 0.01 V and 0.9 V sample.

The binding energies of N 1s and F 1s peaks for the pristine LiTDI salt are ~399 and ~688 eV, respectively as presented in *Figure 12*. After the electrochemical cycling at rather low potential, the LiTDI decomposed as new N 1s and F 1s features are observed at ~400.8 and ~685 eV (LiF). The relative amounts of these decomposition products are rather low compared to the LiTDI salt as both the peak areas are smaller.

4.3 Silicon paper electrode

Copper foil, which has rather high density, is commonly used as current collector for anodes in lithium-ion batteries. The high weight of this electrochemical inactive material significantly reduces the gravimetric energy density of a battery, and in this section, the properties of the freestanding (copper current collector free) silicon paper electrode as anode for lithium-ion batteries are presented and discussed based on **paper III**. The preparation details are described in battery preparation as well as in the **paper III**.

4.3.1 Physical properties

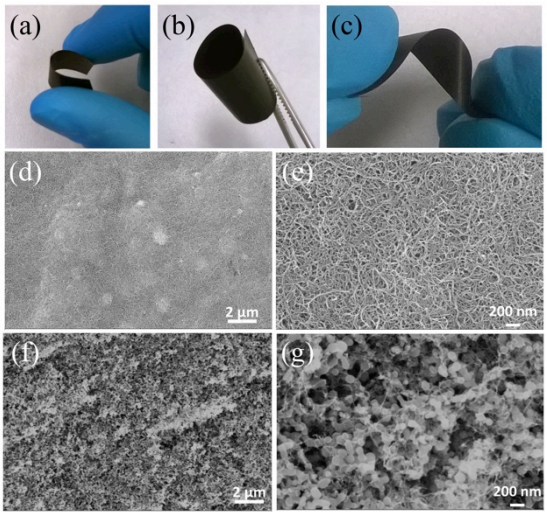

Figure 13. (a, b, c) The flexible silicon electrode under bending and twisting. (d, e) and (f, g) SEM images of the CNT/CNC layer and the SiNP/CNT/CNC layer, respectively.

The paper electrode is ~30 µm in thickness and consists of two layers: the CNT/CNC network as the conductive substrate and SiNP/CNT/CNC as the active material layer. The electrode demonstrates excellent mechanical flexibility and the tensile strength and Young's modulus are 27.4 and 314 MPa, respectively. *Figure 13(a, b and c)* show the electrode under bending and twisting conditions. The surface morphology of the CNT/CNC and the SiNP/CNT/CNC layers are presented as *Figure 13(d, e)* and *(f, g)*, respectively. As the diameters of the CNT and CNC are both ~10 nm, it is difficult to distinguish between these two components in the SEM images. A rather smooth surface is shown for the CNT/CNC sample while the surface is rougher with the presence of silicon nano-powders, which has an average particle size of ~50 nm. FT-IR and Raman results presented in **paper III**

also confirmed the successful synthesis of the composite SiNP/CNT/CNC electrode.

4.3.2 Electrochemical characterizations

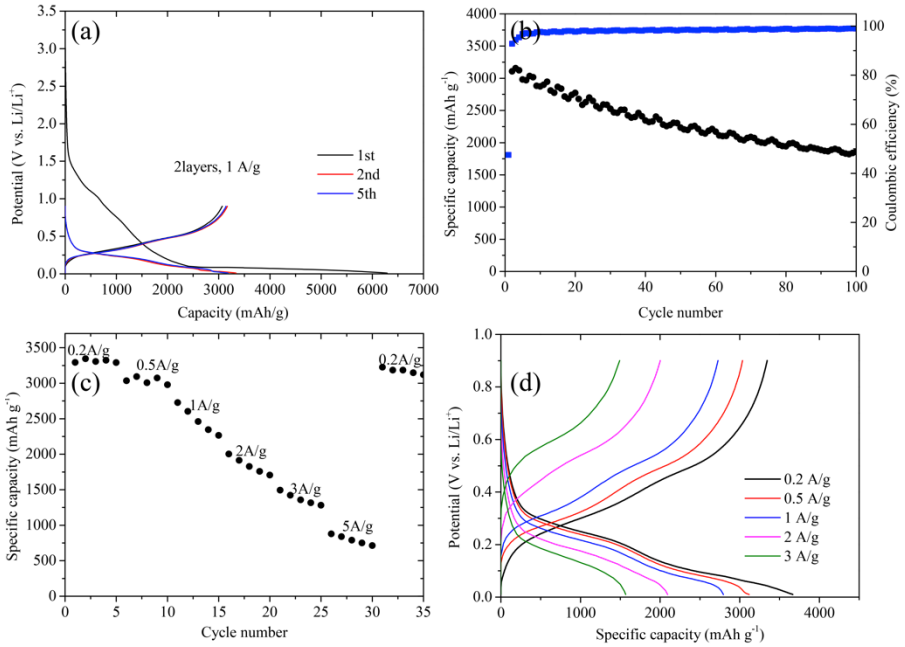

Figure 14. Long-term cycling ((a) potential profile for the 1st, 2nd and 5th cycle (b) specific capacity and coulombic efficiency) and rate capability performance ((c) capacity at different current densities (d) potential curve at different current densities) of the flexible silicon electrode, respectively.

Galvanostatic cycling with a current density of 1 A/g Si between 0.01 V and 0.9 V was carried out to investigate the long-term performance of the free-standing silicon electrode. As shown in *Figure 14(a)*, large irreversible capacity, i.e. low coulombic efficiency, is observed for the first electrochemical cycle as the capacities of discharge (lithiation) and charge (delithiation) processes are 6290 and 3070 mAh/g (based on Si), respectively. This low coulombic efficiency is most likely due to the formation of SEI on the silicon particles as well as the CNT/CNC conductive substrate. Nevertheless, the capacity after 100 cycles (1840 mAh/g, based on Si) was found to be retained at 67% of the capacity achieved for the second cycle, showing a rather good long-term cycling performance. As large volume change is expected with the cycling condition used, the results prove the importance of the CNT/CNC network in achieving good SiNP adhesion and mechanical stability of the electrode. Rate capability tests were performed with current densities of 0.2, 0.5, 1, 2, 3 and 5 A/g, respectively, and the results are

shown in *Figure 14*(c, d). The average capacity achieved with a 0.2 A/g current density was ~3250 mAh/g and it decreased as the current density increased. However, when the current density was changed to 0.2 A/g after the cycling at different current densities, the capacity was increased back to ~3200 mAh/g, indicating a good capacity retention and rate capability.

5. Conclusions and future work

This thesis presents the investigation of the interfacial chemistry on the silicon electrodes with FEC as electrolyte as additive and LiTDI salt-based electrolyte, respectively, using photoelectron spectroscopy as the main characterization technique. The facile synthesis as well as the electrochemical performance of the flexible and freestanding silicon paper electrode is also demonstrated.

Fluoroethylene carbonate is well-know electrolyte additive for alloy-type anode materials, especially silicon, to improve coulombic efficiency and capacity retention. The galvanostatic cycling performed on the silicon half-cells using FEC/LP40 and LP40 electrolytes confirmed the effectiveness of the FEC additive, as the long-term cycling was substantially improved with 10 wt% of FEC in the LP40 electrolyte compared to LP40-only electrolyte. It is found that the FEC additive decomposes prior to other electrolyte solvents, and forms a conformal and stable SEI layer, which limits further electrolyte solvent decomposition. This SEI layer well prevented the emergence of cracks and preserved the void structures of the silicon electrode. The non-destructive PES depth profiling shows the SEI mainly consists of the FEC decomposition products, such as LiF, -CHF-OCO_2- type compounds, etc.

LiTDI has been investigated as an alternative lithium salt to the widely used $LiPF_6$ in the electrolyte for silicon electrodes. Large irreversible capacity during the first electrochemical cycle was observed, indicating significant SEI formation. Hard X-ray photoelectron spectroscopy (HAXPES) was used to study the composition of the SEI layer, which was found mainly to contain hydrocarbon, ether-type and carbonate-type species. Salt decomposition was also observed, but no detrimental effect towards the active silicon material was noticed, showing a good stability with silicon electrodes.

Since the use of the heavy weight copper current collector for the anode significantly reduces the specific energy density, a freestanding (Cu current collector free) silicon paper electrode is developed using a facile synthesis approach. The electrode consists of two layers: CNC/CNT as the conductive substrate and SiNPs/CNC/CNT as the active material layer, and the obtained flexible electrode shows good mechanical properties. Although the irreversible capacity was large (~51 %), rather good long-term capacity retention (67 % of the capacity obtained for the second cycle) was achieved after 100 cycles. Promising rate capability was observed as a capacity of ~800 mAh/g (based on the silicon weight) even at a current density of 5 A/g.

The present work shows the promise of the silicon anode with compatible electrode formulation, electrolyte composition and cycling conditions. Further work will be devoted on optimizing these aspects for the silicon anode. The study on lithium iron silicon cathode has not been a focus in this thesis work, but more work needs to be done for the cathode in order to achieve good performance of the ‘‘all silicon lithium-ion batteries’’. Besides, the understanding of the interfacial chemistry on the silicon electrodes, especially the SiO_2/Si surface chemistry, is essential and still needs more work. It is also important to explore different characterization techniques so that more comprehensive information can be obtain in the studies.

6. Sammanfattning på svenska

Olika teknologier för elektrokemisk energilagring såsom bly-syra-, nickel-kadmium-, nickel-metallhydrid- och litiumjonbatterier utnyttjas i såväl portabel elektronik som elfordon. Bland dessa tillgängliga teknologier har litiumjonbatterier stora fördelar vad gäller specifik energidensitet både i avseende på vikt och volym gentemot de andra teknologierna. Sedan Sonys lansering av litiumjonbatterier 1991 så har en förbättring av prestandan hos denna teknologi pågått kontinuerligt genom utvecklandet av nya elektrodmaterial, nya elektrolyter samt optimering av elektrodformuleringen, dessutom har en avsevärd mängd forskning lagts på förståelse för de grundläggande mekanismerna som sker i litiumjonbatterier för att ta utvecklingen ett steg längre.

Syftet med projektet är att utveckla ett fungerande batteri med kiselbaserade elektroder, genom användandet av litiumjärnsilikat som katodmaterial och rent kisel som anod. Både litium-järnsilikatet med sina ~330 mAh/g, om man räknar två litiumjoner per formelenhet, och kisel med ~3600 mAh/g har högre teoretisk kapacitet än dagens vanligaste kommersiella material, koboltoxid och grafit, som ligger på ~160 mAh/g och ~360 mAh/g respektive. En övergång till järnsilikat och kisel som elektrodmaterial skulle öka den specifika energin i batterierna. Dessutom finns goda möjligheter till att minska kostnaden för batterier genom användandet av kiselbaserade elektroder, eftersom kisel är ett av de vanligaste förekommande grundämnena på jorden.

Fokus i detta arbete har legat på att förbättra prestandan i den rena kiselanoden samt förstå elektrodens funktion under drift. Ett allvarligt problem med kiselbaserade batterier är att deras prestanda försämras relativt snabbt på grund av de stora volymsförändringar som elektroden genomgår vid den legering mellan litium och kisel som sker under cykling. Det passiverande gränsskiktet mellan elektrod och elektrolyt, även kallat SEI från engelskans Solid Electrolyte Interphase, utsätts för stora mekaniska påfrestningar på grund av volymsförändringen. I detta arbete undersöktes inverkan av fluoroetylenkarbonat (FEC) som elektrolyttillsats i en karbonatbaserad standardelektrolyt med litiumhexafostat som salt (LP40). En signifikant förbättring av batteriets prestanda kunde uppnås. Undersökningar av ytmorfologin visade att denna förbättring beror på att FEC kan begränsa den kontinuerliga elektrolytnedbrytningen och uppkomsten av sprickor i elektroden. Detta genom bildandet av ett stabilt SEI lager som till största del består av ned-

brytningsprodukter från FEC, såsom litiumfluorid och fluorerade kolväten innehållande en karbonatgrupp (-CHF-OCO_2-). Den föreslagna mekanismen för detta illustreras i figur 1. Resultaten visar hur viktigt ett stabilt SEI lager är, såväl som optimeringen av elektrolytens sammansättning.

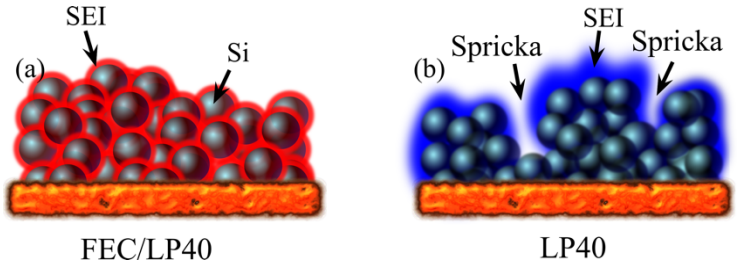

Figur 1. Schematisk illustration av de olika SEI lagren som bildas på en kiselelektrod under elektrokemisk cykling i en karbonatbaserad standard elektrolyt (LP40) med FEC (a), och utan FEC (b) i elektrolyten.

I denna studie har även ett alternativt salt till elektrolyten för tillämpningar med kiselelektroder blivit undersökt. Den Coulombiska verkningsgraden för den första cykeln var relativt låg (44.4%), vilket huvudsakligen tillskrivs bildandet av ett SEI lager bestående mestadels av kolväten av eter- och karbonattyp.

Utöver detta studerades även flexibla kiselelektroder beredda av kiselnanopulver, *Cladophora* nanocellulosa, och kolnanorör via en okomplicerad vakuumfiltrering. Goda mekaniska egenskaper i form av stabilitet och flexibilitet uppvisades, vilket kommer vara vitalt för att uppnå bra prestanda i olika portabla elektroniska enheter. Även om den initiala kapacitetsförlusten var stor så visade fortsatt cykling på god stabilitet över ett intervall på 100 cykler. 67 % av den andra cykelns kapacitet bibehölls vid försökets slut och en kapacitet på ~800mAh/g uppmättes vid en strömtäthet på 5 A/g, räknat på kiselelektroden.

7. Acknowledgements

First and foremost, I would like to thank my main supervisor, Torbjörn Gustafsson, for giving me the opportunity to work on this project, and all the support inside as well as outside of the academic work. Thank you for always trusting me as an independent researcher and keeping me rigorous and patient during my study.

I would like to thank my co-supervisors, Kristina Edström and Daniel Brandell, for all the fruitful discussions and your advices. Special thanks to Maria Hahlin for introducing me to the fascinating world of XPS. I would like to acknowledge Leif Nyholm for sharing your knowledge of electrochemistry. Thanks to Fredrik Björefors, not only for your instructive feedback of my work, but also including me as lab teacher in your course. It was a great experience and lots of fun to teach with you.

I would like to also thank my talented collaborators: Bing Sun, Fredrik Lindgren, Bertrand Philippe, Zhaohui Wang and Julia Maibach. Your creative ideas and meticulous experimental work carried me and this work would never be possible without your contribution. Special thanks to Bing, you taught me building the very first battery in my life and always supported me.

I would like to acknowledge all the ‘‘synchrotron team’’ members for bringing fun as well as being supportive during the synchrotron beam times: Maria, Julia, Bertrand, Reza Younesi, Tim Nordh, Katarzyna Ciosek Högström, Sara Malmgren, Burak Aktekin and Erik Björklund. Mihaela Gorgoi, thank you for always keeping the beamline well-functioning.

It is my great pleasure to share our office with you, Andreas Bildberg and Tim. I would like to thank you both for helping me out on scientific issues, life outside of work as well as Swedish. Thanks a lot to Jia Liu for always sharing positive attitudes and keeping me in a good mentality.

I would also like to acknowledge Henrik Eriksson for your technical support in the lab. Special thanks to Tatti and Eva for helping me with all the administrative issues.

Many thanks to my colleagues and friends at the Ångström Laboratory: Adam, Alina, Anti, Bing Cai, Cesar, Charlotte, Chenjuan, David, Fabian, Fang, Gabi, Girma, Jeff, Jonas Mindemark, Linus, Mario, Matt, Mohammed, Richard, Ruijun, Sara Munktell, Solveig, Shruti, Shuainan and Peng, Stéven, Viktor, Wei Wei, Yiming, Yuxia, Yu Zhang, Yue Ma, and Zhen Qiu, for all the delightful discussions, coffee breaks and after-works.

Special thanks to my friends for all the wonderful ‘‘Sanguosha’’ time we had together: Bing S., Bing C. & Kenneth, Chenjuan, Jia, Yang, Yiming, Yuan, Yue and Zhaohui. Thanks to my friends back in China, especially Zheng Qian, for always sharing happiness and cheering me up.

Last but not least, I would like to thank my parents for always trusting and supporting me in every aspect. I would also like to thank my sister and brother in law for bringing laughter and looking after our parents. I love you all.

References

(1) B. J. Landi, M. J. Ganter, C. D. Cress, R. A. DiLeo and R. P. Raffaelle, *Energy Environ. Sci.*, 2009, **2**, 638–654.
(2) T. Nagaura and K. Tozawa, Lithium ion rechargeable battery, *Prog. Batteries Solar Cells*, 1990.
(3) Y. Nishi, *J. Power Sources*, 2001, **100**, 101–106.
(4) K. Mizushima, Jones, P. C., P. J. Wiseman and J. B. Goodenough, *Mater. Res. Bull.*, 1980, **15**, 783–789.
(5) T. Ohzuku and A. Ueda, *J. Electrochem. Soc.*, 1994, **141**, 2972–2977.
(6) C.-H. Doh, D.-H. Kim, H.-S. Kim, H.-M. Shin, Y.-D. Jeong, S.-I. Moon, B.-S. Jin, S. W. Eom, H.-S. Kim, K.-W. Kim, D.-H. Oh and A. Veluchamy, *J. Power Sources*, 2008, **175**, 881–885.
(7) D. Belov and M.-H. Yang, *J. Solid State Electrochem.*, 2007, **12**, 885–894.
(8) N. Yabuuchi and T. Ohzuku, *J. Power Sources*, 2003, **119-121**, 171–174.
(9) S. Albrecht, J. Kümpers, M. Kruft, S. Malcus, C. Vogler, M. Wahl and M. Wohlfahrt-Mehrens, *J. Power Sources*, 2003, **119-121**, 178–183.
(10) M. S. Whittingham, *Chem. Rev.*, 2014, **114**, 11414–11443.
(11) Z. Lu, L. Y. Beaulieu, R. A. Donaberger, C. L. Thomas and J. R. Dahn, *J. Electrochem. Soc.*, 2002, **149**, A778.
(12) M. M. Thackeray, S.-H. Kang, C. S. Johnson, J. T. Vaughey, R. Benedek and S. A. Hackney, *J. Mater. Chem.*, 2007, **17**, 3112.
(13) F. Zhou, X. Zhao, A. van Bommel, X. Xia and J. R. Dahn, *J. Electrochem. Soc.*, 2011, **158**, A187.
(14) M. M. Thackeray, P. J. Johnson, L. A. de Picciotto, P. G. Bruce and J. B. Goodenough, *Mater. Res. Bull.*, 1984, **19**, 179–187.
(15) J. M. Tarascon, E. Wang, F. K. Shokoohi, W. R. McKinnon and S. Colson, *J. Electrochem. Soc.*, 1991, **138**, 2859–2864.
(16) R. J. Gummow, A. de Kock and M. M. Thackeray, *Solid State Ionics*, 1994, **69**, 59–67.
(17) R. Santhanam and B. Rambabu, *J. Power Sources*, 2010, **195**, 5442–5451.
(18) Q. Zhong, A. Bonakdarpour, M. Zhang, Y. Gao and J. R. Dahn, *J. Electrochem. Soc.*, 1997, **144**, 205–213.
(19) A. K. Padhi, K. S. Nanjundaswamy and J. B. Goodenough, *J. Electrochem. Soc.*, 1997, **144**, 1188–1194.

(20) A. K. Padhi, K. S. Nanjundaswamy, C. Masquelier, S. Okada and J. B. Goodenough, *J. Electrochem. Soc.*, 1997, **144**, 1609–1613.
(21) A. Yamada, S. C. Chung and K. Hinokuma, *J. Electrochem. Soc.*, 2001, **148**, A224.
(22) S. Y. Chung, J. T. Bloking and Y. M. Chiang, *Nat. Mater.*, 2002, **1**, 123–128.
(23) H. Huang, S. C. Yin and L. F. Nazar, *Electrochem. Solid-State Lett.*, 2001, **4**, A170.
(24) A. Nytén, A. Abouimrane, M. Armand, T. Gustafsson and J. O. Thomas, *Electrochem. Commun.*, 2005, **7**, 156–160.
(25) A. Nytén, S. Kamali, L. Häggström, T. Gustafsson and J. O. Thomas, *J. Mater. Chem.*, 2006, **16**, 2266–2272.
(26) S.-I. Nishimura, S. Hayase, R. Kanno, M. Yashima, N. Nakayama and A. Yama-da, *J. Am. Chem. Soc.*, 2008, **130**, 13212–13213.
(27) C. Sirisopanaporn, A. Boulineau, D. Hanzel, R. Dominko, B. Budic, A. R. Armstrong, P. G. Bruce and C. Masquelier, *Inorg. Chem.*, 2010, **49**, 7446–7451.
(28) L.-L. Zhang, S. Duan, X.-L. Yang, G. Peng, G. Liang, Y.-H. Huang, Y. Jiang, S.-B. Ni and M. Li, *ACS Appl. Mater. Interfaces*, 2013, **5**, 12304–12309.
(29) H. Zhu, X. Wu, L. Zan and Y. Zhang, *Electrochim. Acta*, 2014, **117**, 34–40.
(30) M. Dahbi, S. Urbonaite and T. Gustafsson, *J. Power Sources*, 2012, **205**, 456–462.
(31) R. Dominko, D. E. Conte, D. Hanzel, M. Gaberscek and J. Jamnik, *J. Power Sources*, 2008, **178**, 842–847.
(32) Y. Xu, W. Shen, C. Wang, A. Zhang, Q. Xu, H. Liu, Y. Wang and Y. Xia, *Electrochim. Acta*, 2015, **167**, 340–347.
(33) L. Qu, Y. Liu, S. Fang, L. Yang and S.-I. Hirano, *Electrochim. Acta*, 2015, **163**, 123–131.
(34) D. Ensling, M. Stjerndahl, A. Nytén, T. Gustafsson and J. O. Thomas, *J. Mater. Chem.*, 2009, **19**, 82–88.
(35) A. Nytén, M. Stjerndahl, H. Rensmo, H. Siegbahn, M. Armand, T. Gustafsson, K. Edström and J. O. Thomas, *J. Mater. Chem.*, 2006, **16**, 3483–3488.
(36) C. Dippel, S. Krueger, R. Kloepsch, P. Niehoff, B. Hoffmann, S. Nowak, S. Passerini, M. Winter and J. Li, *Electrochim. Acta*, 2012, **85**, 66–71.
(37) R. J. Gummow and Y. He, *J. Power Sources*, 2014, **253**, 315–331.
(38) A. Kokalj, R. Dominko, G. Mali, A. Meden, M. Gaberšček and J. Jamnik, *Chem. Mater.*, 2007, **19**, 3633–3640.
(39) A. Saracibar, Z. Wang, K. J. Carroll, Y. S. Meng and M. E. A.-D. Dompablo, *J. Mater. Chem. A*, 2015, **3**, 6004–6011.
(40) Z. L. Gong, Y. X. Li and Y. Yang, *Electrochem. Solid-State Lett.*, 2006, **9**, A542.

(41) R. Fong, U. von Sacken and J. R. Dahn, *J. Electrochem. Soc.*, 1990, **137**, 2009–2013.
(42) K. Edström, M. Herstedt and D. P. Abraham, *J. Power Sources*, 2006, **153**, 380–384.
(43) K. M. Colbow, J. R. Dahn and R. R. Haering, *J. Power Sources*, 1989, **26**, 397–402.
(44) K. Zaghib, M. Simoneau, M. Armand and M. Gauthier, *J. Power Sources*, 1999, **81–82**, 300–305.
(45) I. Belharouak, G. M. Koenig, T. Tan, H. Yumoto, N. Ota and K. Amine, *J. Electrochem. Soc.*, 2012, **159**, A1165–A1170.
(46) K. Wu, J. Yang, Y. Zhang, C. Wang and D. Wang, *J. Appl. Electrochem.*, 2012, **42**, 989–995.
(47) Y.-B. He, B. Li, M. Liu, C. Zhang, W. Lv, C. Yang, J. Li, H. Du, B. Zhang, Q.-H. Yang, J.-K. Kim and F. Kang, *Sci. Rep.*, 2012, 2.
(48) A. N. Dey, *J. Electrochem. Soc.*, 1971, **118**, 1547–1549.
(49) M. N. Obrovac and V. L. Chevrier, *Chem. Rev.*, 2014, **114**, 11444–11502.
(50) W.-J. Zhang, *J. Power Sources*, 2011, **196**, 13–24.
(51) W.-J. Zhang, *J. Power Sources*, 2011, **196**, 877–885.
(52) C. J. Wen and R. A. Huggins, *J. Solid State Chem.*, 1981, **37**, 271–278.
(53) R. A. Sharma and R. N. Seefurth, *J. Electrochem. Soc.*, 1976, **123**, 1763–1768.
(54) A. M. Wilson and J. R. Dahn, *J. Electrochem. Soc.*, 1995, **142**, 326–332.
(55) P. Limthongkul, Y.-I. Jang, N. J. Dudney and Y.-M. Chiang, *Acta Mater.*, 2003, **51**, 1103–1113.
(56) M. N. Obrovac and L. Christensen, *Electrochem. Solid-State Lett.*, 2004, **7**, A93–A96.
(57) M. N. Obrovac and L. J. Krause, *J. Electrochem. Soc.*, 2007, **154**, A103–A103.
(58) J. H. Ryu, J. W. Kim, Y.-E. Sung and S. M. Oh, *Electrochem. Solid-State Lett.*, 2004, **7**, A306–A306.
(59) U. Kasavajjula, C. Wang and A. J. Appleby, *J. Power Sources*, 2007, **163**, 1003–1039.
(60) H. Li, X. Huang, L. Chen, Z. Wu and Y. Liang, *Electrochem. Solid-State Lett.*, 1999, **2**, 547–549.
(61) M. Holzapfel, H. Buqa, W. Scheifele, P. Novák and F.-M. Petrat, *Chem. Commun.*, 2005, 1566–1568.
(62) H. Kim, M. Seo, M. H. Park and J. Cho, *Angew. Chem. Int. Ed.*, 2010, **49**, 2146–2149.
(63) M. Gu, Y. Li, X. Li, S. Hu, X. Zhang, W. Xu, S. Thevuthasan, D. R. Baer, J.-G. Zhang, J. Liu and C. Wang, *ACS Nano*, 2012, **6**, 8439–8447.

(64) M. T. McDowell, I. Ryu, S. W. Lee, C. Wang, W. D. Nix and Y. Cui, *Adv. Mater.*, 2012, **24**, 6034–6041.
(65) I. Ryu, J. W. Choi, Y. Cui and W. D. Nix, *J. Mech. Phys. Solids*, 2011, **59**, 1717–1730.
(66) Y. Oumellal, N. Delpuech, D. Mazouzi, N. Dupré, J. Gaubicher, P. Moreau, P. Soudan, B. Lestriez and D. Guyomard, *J. Mater. Chem.*, 2011, **21**, 6201–6208.
(67) N. S. Hochgatterer, M. R. Schweiger, S. Koller, P. R. Raimann, T. Wöhrle, C. Wurm and M. Winter, *Electrochem. Solid-State Lett.*, 2008, **11**, A76–A80.
(68) J. S. Bridel, T. Azaïs, M. Morcrette, J. M. Tarascon and D. Larcher, *Chem. Mater.*, 2010, **22**, 1229–1241.
(69) J. Li, R. B. Lewis and J. R. Dahn, *Electrochem. Solid-State Lett.*, 2007, **10**, A17–A20.
(70) A. Magasinski, B. Zdyrko, I. Kovalenko, B. Hertzberg, R. Burtovyy, C. F. Huebner, T. F. Fuller, I. Luzinov and G. Yushin, *ACS Appl. Mater. Interfaces*, 2010, **2**, 3004–3010.
(71) S. Komaba, K. Shimomura, N. Yabuuchi, T. Ozeki, H. Yui and K. Konno, *J. Phys. Chem. C*, 2011, **115**, 13487–13495.
(72) I. Kovalenko, B. Zdyrko, A. Magasinski, B. Hertzberg, Z. Milicev, R. Burtovyy, I. Luzinov and G. Yushin, *Science*, 2011, **334**, 75–79.
(73) J. Liu, Q. Zhang, Z.-Y. Wu, J.-H. Wu, J.-T. Li, L. Huang and S.-G. Sun, *Chem. Commun.*, 2014, **50**, 6386.
(74) D. Mazouzi, B. Lestriez, L. Roué and D. Guyomard, *Electrochem. Solid-State Lett.*, 2009, **12**, A215–A218.
(75) D. Mazouzi, Z. Karkar, C. Reale Hernandez, P. Jimenez Manero, D. Guyomard, L. Roué and B. Lestriez, *J. Power Sources*, 2015, **280**, 533–549.
(76) C. K. Chan, R. Ruffo, S. S. Hong and Y. Cui, *J. Power Sources*, 2009, **189**, 1132–1140.
(77) B. Philippe, R. Dedryvère, J. Allouche, F. Lindgren, M. Gorgoi, H. Rensmo, D. Gonbeau and K. Edström, *Chem. Mater.*, 2012, **24**, 1107–1115.
(78) M. Nie, D. P. Abraham, Y. Chen, A. Bose and B. L. Lucht, *J. Phys. Chem. C*, 2013, **117**, 13403–13412.
(79) S. P. V. Nadimpalli, V. A. Sethuraman, S. Dalavi, B. L. Lucht, M. J. Chon, V. B. Shenoy and P. R. Guduru, *J. Power Sources*, 2012, **215**, 145–151.
(80) B. Philippe, R. Dedryvère, M. Gorgoi, H. Rensmo, D. Gonbeau and K. Edström, *Chem. Mater.*, 2013, **25**, 394–404.
(81) B. Philippe, R. Dedryvère, M. Gorgoi, H. Rensmo, D. Gonbeau and K. Edström, *J. Am. Chem. Soc.*, 2013, **135**, 9829–9842.
(82) H. Nakai, T. Kubota, A. Kita and A. Kawashima, *J. Electrochem. Soc.*, 2011, **158**, A798–A798.

(83) S. Dalavi, P. Guduru and B. L. Lucht, *J. Electrochem. Soc.*, 2012, **159**, A642–A646.
(84) Y.-M. Lin, K. C. Klavetter, P. R. Abel, N. C. Davy, J. L. Snider, A. Heller and C. B. Mullins, *Chem. Commun.*, 2012, **48**, 7268–7270.
(85) S.-H. Ng, J. Wang, D. Wexler, K. Konstantinov, Z.-P. Guo and H.-K. Liu, *Angew. Chem. Int. Ed.*, 2006, **45**, 6896–6899.
(86) S. H. Ng, J. Wang, D. Wexler and S. Y. Chew, *J. Phys. Chem. C*, 2007, **111**, 11131–11138.
(87) R. Huang, X. Fan, W. Shen and J. Zhu, *Appl. Phys. Lett.*, 2009, **95**, 133119.
(88) N. Dimov, S. Kugino and M. Yoshio, *Electrochim. Acta*, 2003, **48**, 1579–1587.
(89) O. Park, J.-I. Lee, M.-J. Chun, J.-T. Yeon, S. Yoo, S. Choi, N.-S. Choi and S. Park, *RSC Adv.*, 2013, **3**, 2538–2542.
(90) F.-H. Du, B. Li, W. Fu, Y.-J. Xiong, K.-X. Wang and J.-S. Chen, *Adv. Mater.*, 2014, **26**, 6145–6150.
(91) Y. Yao, N. Liu, M. T. McDowell, M. Pasta and Y. Cui, *Energy Environ. Sci.*, 2012, **5**, 7927–7930.
(92) A. Touidjine, M. Morcrette, M. Courty, C. Davoisne, M. Lejeune, N. Mariage, W. Porcher and D. Larcher, *J. Electrochem. Soc.*, 2015, **162**, A1466–A1475.
(93) M. V. Reddy, T. Yu, C. H. Sow, Z. X. Shen, C. T. Lim, G. V. Subba Rao and B. V. R. Chowdari, *Adv. Funct. Mater.*, 2007, **17**, 2792–2799.
(94) X. Zhu, Y. Zhu, S. Murali, M. D. Stoller and R. S. Ruoff, *ACS Nano*, 2011, **5**, 3333–3338.
(95) G. Zhou, D.-W. Wang, F. Li, L. Zhang, N. Li, Z.-S. Wu, L. Wen, G. Q. M. Lu and H.-M. Cheng, *Chem. Mater.*, 2010, **22**, 5306–5313.
(96) W.-M. Zhang, X.-L. Wu, J.-S. Hu, Y.-G. Guo and L.-J. Wan, *Adv. Funct. Mater.*, 2008, **18**, 3941–3946.
(97) L. Li, A.-R. O. Raji and J. M. Tour, *Adv. Mater.*, 2013, **25**, 6298–6302.
(98) H. Xia, M. Lai and L. Lu, *J. Mater. Chem.*, 2010, **20**, 6896–6902.
(99) M. N. Obrovac, R. A. Dunlap, R. J. Sanderson and J. R. Dahn, *J. Electrochem. Soc.*, 2001, **148**, A576–A588.
(100) K. Xu, *Chem. Rev.*, 2004, **104**, 4303–4418.
(101) J. Y. Song, Y. Y. Wang and C. C. Wan, *J. Power Sources*, 1999, **77**, 183–197.
(102) J. W. Fergus, *J. Power Sources*, 2010, **195**, 4554–4569.
(103) K. Murata, S. Izuchi and Y. Yoshihisa, *Electrochim. Acta*, 2000, **45**, 1501–1508.
(104) A. Lewandowski and A. Świderska-Mocek, *J. Power Sources*, 2009, **194**, 601–609.
(105) K. Xu, *Chem. Rev.*, 2014, **114**, 11503–11618.

(106) D. Aurbach, B. Markovsky, A. Shechter, Y. Ein Eli and H. Cohen, *J. Electrochem. Soc.*, 1996, **143**, 3809–3820.
(107) S. Shui Zhang, *Electrochem. Commun.*, 2006, **8**, 1423–1428.
(108) Z. Chen, J. Liu and K. Amine, *Electrochem. Solid-State Lett.*, 2007, **10**, A45–A47.
(109) Z. Chen, J. Liu, A. N. Jansen, G. GirishKumar, B. Casteel and K. Amine, *Electrochem. Solid-State Lett.*, 2010, **13**, A39–A42.
(110) L. Li, S. Zhou, H. Han, H. Li, J. Nie, M. Armand, Z. Zhou and X. Huang, *J. Electrochem. Soc.*, 2011, **158**, A74–A82.
(111) L. Niedzicki, M. Kasprzyk, K. Kuziak, G. Z. Żukowska, M. Marcinek, W. Wieczorek and M. Armand, *J. Power Sources*, 2011, **196**, 1386–1391.
(112) L. Niedzicki, E. Karpierz, A. Bitner, M. Kasprzyk, G. Z. Zukowska, M. Marcinek and W. Wieczorek, *Electrochim. Acta*, 2013, **117**, 224–229.
(113) J. Liu, Z. Chen, S. Busking and K. Amine, *Electrochem. Commun.*, 2007, **9**, 475–479.
(114) L. Martin, H. Martinez, M. Ulldemolins, B. Pecquenard and F. Le Cras, *Solid State Ionics*, 2012, **215**, 36–44.
(115) M. Ulldemolins, F. Le Cras, B. Pecquenard, V. P. Phan, L. Martin and H. Mar-tinez, *J. Power Sources*, 2012, **206**, 245–252.
(116) H. Shin, J. Park, A. M. Sastry and W. Lu, *J. Electrochem. Soc.*, 2015, **162**, A1683–A1692.
(117) Z.-C. Wang, J. Xu, W.-H. Yao, Y.-W. Yao and Y. Yang, *ECS Transactions*, 2012, **41**, 29–40.
(118) S. Dalavi, M. Xu, B. Knight and B. L. Lucht, *Electrochem. Solid-State Lett.*, 2011, **15**, A28–A31.
(119) C. Täubert, M. Fleischhammer, M. Wohlfahrt-Mehrens, U. Wietelmann and T. Buhrmester, *J. Electrochem. Soc.*, 2010, **157**, A721–A728.
(120) Q. Wu, W. Lu, M. Miranda, T. K. Honaker-Schroeder, K. Y. Lakhsassi and D. Dees, *Electrochem. Commun.*, 2012, **24**, 78–81.
(121) Y. Zhu, Y. Li, M. Bettge and D. P. Abraham, *J. Electrochem. Soc.*, 2012, **159**, A2109–A2117.
(122) M. Adachi, *J. Electrochem. Soc.*, 1999, **146**, 1256–1261.
(123) C. Buhrmester, L. Moshurchak, R. L. Wang and J. R. Dahn, *J. Electrochem. Soc.*, 2006, **153**, A288–A294.
(124) X. L. Yao, S. Xie, C. H. Chen, Q. S. Wang, J. H. Sun, Y. L. Li and S. X. Lu, *J. Power Sources*, 2005, **144**, 170–175.
(125) K. Ciosek Högström, H. Lundgren, S. Wilken, T. G. Zavalis, M. Behm, K. Edström, P. Jacobsson, P. Johansson and G. Lindbergh, *J. Power Sources*, 2014, **256**, 430–439.
(126) H. Bryngelsson, M. Stjerndahl, T. Gustafsson and K. Edström, *J. Power Sources*, 2007, **174**, 970–975.

(127) P. Verma, P. Maire and P. Novák, *Electrochim. Acta*, 2010, **55**, 6332–6341.
(128) S. Malmgren, K. Ciosek, R. Lindblad, S. Plogmaker, J. Kühn, H. Rensmo, K. Edström and M. Hahlin, *Electrochim. Acta*, 2013, **105**, 83–91.
(129) A. M. Andersson and K. Edström, *J. Electrochem. Soc.*, 2001, **148**, A1100–A1100.
(130) S. Leroy, F. Blanchard, R. Dedryvère, H. Martinez, B. Carré, D. Lemordant and D. Gonbeau, *Surf. Interface Anal.*, 2005, **37**, 773–781.
(131) A. Tokranov, B. W. Sheldon, C. Li, S. Minne and X. Xiao, *ACS Appl. Mater. Interfaces*, 2014, **6**, 6672–6686.
(132) E. Peled, D. Bar Tow, A. Merson, A. Gladkich, L. Burstein and D. Golodnitsky, *J. Power Sources*, 2001, **97-98**, 52–57.
(133) K. W. Schroder, A. G. Dylla, S. J. Harris, L. J. Webb and K. J. Stevenson, *ACS Appl. Mater. Interfaces*, 2014, **6**, 21510–21524.
(134) V. Etacheri, O. Haik, Y. Goffer, G. A. Roberts, I. C. Stefan, R. Fasching and D. Aurbach, *Langmuir*, 2012, **28**, 965–976.
(135) I. A. Profatilova, C. Stock, A. Schmitz, S. Passerini and M. Winter, *J. Power Sources*, 2013, **222**, 140–149.
(136) Z. Wang, C. Xu, P. Tammela, J. Huo, M. Strømme, K. Edström, T. Gustafsson and L. Nyholm, *J. Mater. Chem. A*, 2015, **3**, 14109–14115.
(137) C. Xu, F. Lindgren, B. Philippe, M. Gorgoi, F. Björefors, K. Edström and T. Gustafsson, *Chem. Mater.*, 2015, **27**, 2591–2599.
(138) K. Ciosek Högström, S. Malmgren, M. Hahlin, M. Gorgoi, L. Nyholm, H. Rensmo and K. Edström, *Electrochim. Acta*, 2014, **138**, 430–436.